Masters Program in Geospatial Technologies

EXPLORING THE IMPACT OF URBAN GROWTH ON LAND SURFACE TEMPERATURE OF KATHMANDU VALLEY, NEPAL

Sushil Thapa

Dissertation submitted in partial fulfilment of the requirements
for the Degree of *Master of Science in Geospatial Technologies*

NOVA IMS Information Management School
UNIVERSITAT JAUME·I
Westfälische Wilhelms-Universität Münster

EXPLORING THE IMPACT OF URBAN GROWTH ON LAND SURFACE TEMPERATURE OF KATHMANDU VALLEY, NEPAL

Dissertation Supervised by

Filiberto Pla Bañón, PhD

Professor, Dept. Lenguajes y Sistemas Informaticos

Universitat Jaume I, Castellón, Spain

Dissertation Co-supervised by

Pedro Cabral, PhD

Professor, Instituto Superior de Estatística e Gestão de Informação

Universidade Nova de Lisboa, Lisbon, Portugal

Edzer Pebesma, PhD

Professor, Institute for Geoinformatics

Westfälische Wilhelms-Universität, Münster, Germany

February 2017

ACKNOWLEDGEMENTS

I am very much delighted to express my profound gratitude to all the generous people for their help and support. My Masters endeavor has been an amazing learning experience and this dissertation would not have been accomplished without them.

First of all, I am very much grateful to my supervisor and co-supervisors: Prof. Dr. Filiberto Pla Banon, Prof. Dr. Pedro Cabral and Prof. Dr. Edzer Pebesma for their valuable suggestions and remarks.

I would like to extend my sincere gratitude to Dr. Pedro Latorre Carmona, Department of Computer Languages and Systems, UJI for his encouragement, guidance and constructive criticisms throughout the project.

I would also greatly acknowledge professors Joaquin Huerta, Christoph Brox, Marco Painho, Michael Gould, Christian Kray for the excellent organization of the Master's Program.

I am highly obliged in taking the opportunity to sincerely thank all my professors from UJI and ifgi who bestowed me with multidisciplinary knowledge and skills and helped to develop professionalism in me.

I am duly grateful to European Commission for granting me with the scholarship to pursue my study here in Europe.

Special thanks to all the administrative staffs from UJI and ifgi who were always kind to me. Thanks to all of my friends for sharing awesome memories.

I also express my sincere gratitude to my parents and brothers for their inspirations, unconditional love and support.

EXPLORING THE IMPACT OF URBAN GROWTH ON LAND SURFACE TEMPERATURE OF KATHMANDU VALLEY, NEPAL

ABSTRACT

Kathmandu is experiencing rapid urban growth since last few decades. Cities are expanding across the countryside at the expense of productive land. Such urban sprawl has incurred adverse environmental consequences affecting quality of life of urban residents in the valley. Recently, Kathmandu has been identified to be on the verge of climate change, especially in the context of urban warming. Thus exploring the impact of urban growth on land surface temperature could be an effective means to unveil environmental issues caused by anthropogenic activities. This can be useful for the urban planners in urban planning and management as well as to raise public awareness regarding urban warming effect. Advancement in thermal Remote Sensing, GIS and statistical procedure has enabled monitoring land surface temperature and its correlation to land use and land cover. To analyze such relationship, we performed supervised classification and change detection to determine the spatial trend of land use and land cover change. After that we obtained the spatial pattern of LST using thermal band of Landsat images. Then we applied regression analysis to explore the relationship between surface temperature and land surface characteristics including both land use land cover types and land use and land cover indices. Based upon our analysis, we found that urban area has increased considerably by 259% during the period 1988-2014. The surface temperatures were found to be greater for bare soil and urban land use types. The regression analysis showed positive correlation between urban growth and LST. Finally we found LULC indices based approach better than LULC class for LST prediction.

KEYWORDS

Land use land cover
Land Surface Temperature
Landsat
Regression analysis
Thermal Remote Sensing
Urban fragmentation
Urban Growth
Urban Heat Island

ACRONYMS

ADB	Asian Development Bank
CBS	Central Bureau of Statistics
CLEAR	Center for Land Use Education and Research
DEM	Digital Elevation Model
DHM	Department of Hydrology and Meteorology
DoR	Department of Roads
GCPs	Ground Control Points
GIS	Geographic Information System
ICIMOD	International Center for Integrated Mountain Development
KRR	Kernel Ridge Regression
LST	Land Surface Temperature
LULC	Land use land cover
NDBI	Normalized Difference Built up Index
NDVI	Normalized Difference Vegetation Index
NDWI	Normalized Difference Water Index
RMSE	Root Mean Square Error
UHI	Urban Heat Island
UNOHCHR	United Nations Office of the High Commissioner for Human Rights
WGS 84	World Geodetic System 84

TABLE OF CONTENTS

Contents

LIST OF TABLES

LIST OF FIGURES

1. INTRODUCTION

1.1 Background & Motivation

Urbanization is nowadays a rising trend globally, especially in an alarming rate in developing countries. This makes cities around the world grow both in number and size. Urban growth is indeed a development process that occurs over some period of time, as city and its suburbs expand into an adjoining countryside. It is primarily accredited to the population growth, as there is a global trend of thousands of people migrating to the cities every year (Bekele, 2005).

Urban growth is characterized by the transformation of natural land covers into built up areas (Rimal, 2011). It causes depletion of greenery in the cities and subsequent increase in the impervious surface. Cities experience unprecedented changes in land use and land cover patterns due to urban growth. As urban growth persists, studies addressing their reciprocal impacts are gaining importance (Parker, 2010). Urban growth has adverse impact on land surface characteristics including its thermal capacity. The increased thermal storage capacity creates so called urban heat island (UHI) effect, observed as an elevated temperature of urban areas relative to rural ones, and it is an important research topic related to urban climate and environmental studies (Stewart & Oke, 2012). UHI emerges through the modification of land surface in a way that favors heat storage and trapping (e.g. reduced vegetation), and anthropogenic heat release from vehicles, industries, and buildings (Oke, 1982; Sailor & Lu, 2004). It is one of the perilous environmental issues, which can cause negative impact on human and environment (Grimmond, 2007). It degrades air, influences local climate, increases ground level ozone production (Lo et al., 2003), and ultimately affects our quality of life. Therefore, the subject of urban growth and UHI has drawn attention from ecologists, urban planners, sociologists, administrators, policy makers, and finally to the urban residents (Bekele, 2005; Li et al., 2012).

Numerous studies related to UHI have been carried out so far (Chen et al., 2006; Coseo et al., 2015; Goward, 1981; Imhoff et al., 2010; Lo et al., 2003; Mirzaei, 2015; Rizwan et al., 2008; Saito et al., 1996; Sun et al., 2012; SRIVANIT et al., 2012; Tan et al., 2010; Tran et al., 2006; Weng et al., 2004; Yuan & Bauer, 2007). These studies cover a wide range of topics related to UHI such as: the influence of urban landscapes and LULC change in UHI phenomenon, spatial-temporal variation of UHI, relationship between UHI and LULC indices, UHI modeling and simulation, impact of UHI effect on heat wave and human welfare, and possible measures to mitigate UHI effect. These studies provide a remarkable contribution to researchers and policy makers concerned with UHI phenomenon.

Land Surface Temperature (LST) is an important parameter in the UHI phenomenon, which manifests high spatial and temporal inhomogeneity especially in urban areas (Zaksek & Ostir, 2011). LST is actually the skin temperature of the land surface which differs from the land surface air temperature (SRIVANIT et al., 2012). It can be derived from freely available data sources such as Landsat, MODIS and ASTER. The thermal band of these sensors enables data collection on thermal properties of the land surface based on the amount of emitted energy. Besides, such data can also be used to monitor LULC change over time. Thus these two prospects enabled researchers to explore the link between LULC change and LST change over time. In this way, monitoring UHI effect due to LULC change has become feasible (Fabrizi et al., 2010).

To obtain LST from thermal images, many algorithms have been proposed such as: Single Channel, Split window, Mono window, Radiative transfer equation etc. (Qin et al., 2001; Yu et al., 2014). However Split window relies on two spectrally adjacent thermal bands, but Landsat 4, 5 and even ETM+ possess only one thermal band. Thus this method is unsuitable for those images. Similarly the problem with the Radiative transfer equation method is that it requires in-situ radio sounding to be launched concurrently with satellite pass. Like Radiative transfer equation method, Mono window method also involves various parameters such as effective mean atmospheric temperature, emissivity and transmittance to be determined, which

requires in-situ measurement. Single Channel method on the other hand requires high quality atmospheric transmittance code to estimate the atmospheric features involved in the model, and is complicated. Therefore, explicitly an image based approach utilizing surface emissivity representing the brightness temperature only, without requiring atmospheric profile parameters has been considered in this study.

Surface emissivity is indispensable for LST inversion, specifically for the image based method. Basically there are three methods to determine the land surface emissivity: Classification based emissivity method, NDVI based method and Temperature independent spectral indices method (Yu et al., 2014). For Classification based emissivity method, surface emissivity is obtained from classification image, but the emissivity value should be known in advance. This requires good knowledge of the study area and emissivity measurement on surface representative of different classes must be coincident with satellite transit time. Temperature independent spectral indices method is also complicated. Hence due to simplicity NDVI based method is suitable for our purpose.

Since LST has a direct link to the land surface characteristics (Quattrochi &Luvall, 1999) and on the other hand, LULC change is strongly related to the urban growth, the study of the relationship between LST and LULC is fundamental to explore the impact of urban growth on land surface temperature, including the UHI effect. The study of the relationship between LST and LULC change helps researchers to understand the cause, spatial-temporal distribution, consequences and possible measures to mitigate the UHI effect.

LULC indices and LULC types are two major indicators of LULC mostly used in the study of LST and LULC relationship. There are various types of LULC indices proposed to investigate the correlations between LULC and LST. Amongst several indices, Normalized Difference Vegetation Index (NDVI), Normalized Difference Built up Index (NDBI) and Normalized Difference Water Index (NDWI) strongly correlate with LST (Chen et al., 2006). These indices are extracted using band ratios of different bands of satellite images. Each of these indices has a unique spectral

response to specific LULC types (Guo et al., 2015). For instance, NDVI is used to monitor vegetation health and predict agricultural production; NDBI is sensitive to built-up areas; and NDWI is used to monitor the water content in vegetation. Thus these indices can also be employed to delineate different LULC types based on appropriate threshold values. NDVI is extensively used in relation to LST; NDBI is used in mapping urban areas whereas NDWI is used to extract water bodies (Ahmed et al., 2013). However, these indices cannot give detailed insight on how urban landscape influences UHI phenomenon. The study of the relationship of LST with the land use classes is restricted. Moreover, LULC types are comparatively more stable than LULC indices over time. Therefore, LULC type has been also used in our study. The combined use of both LULC types and indices is assumed to give better understanding about the LST – LULC relationship. Regression analysis is generally used to explore the relationship between LST and LULC (Coseo & Larsen, 2014; Kim & Guldmann, 2014). The regression analysis and statistical measures are indeed useful to determine the influence degrees of LST within various LULC types (Zhu & Zhang, 2011).

This research studies urban growth in the Kathmandu valley and explores land surface temperature variations among various land use land cover types in the valley. Like other developing countries around the world, urbanization is rampant in Nepal as well. According to ADB/ICIMOD (2006), the rate of urbanization in Nepal accounted 6.6% per annum during 1990s, which was among the highest in the Asia Pacific Region. Kathmandu is the most populated urban region in the country which has been facing rapid urbanization over the decades. Factors responsible for rapid urban growth in the valley are physical conditions of the valley, public service accessibility, employment opportunities, real estate market, population growth, political situation and government plans and policies. By physical conditions, it means that the valley has topography suitable for the residence. Kathmandu being the major economic hub of the country provides employment opportunities and has accessibility to the public services. Major commercials and government agencies are confined within the city core area of the valley. Real estate market is also flourishing in the region whereas government plans and policies in relation to land use are not

much effective. Likewise political turmoil in Nepal due to armed conflict between the state and the then Maoists rebels during the period of 1996 to 2006 caused displacement of many people from various parts of the country to the valley, as it was the most secure place at that time. Besides these factors, construction of Tribhuvan Highway connecting region of India, and Araniko Highway to China increased external influx to the valley. Nepal's first and only international airport, Tribhuvan International Airport, located in the valley also attracted people to the valley (Thapa, 2009; Thapa & Murayama, 2009; DoR, 2004; Sharma, 2003; UN-OHCHR, 2012; Ghimire & Upreti, 2008).

Thus urban growth has been identified as a critical process in the valley. It has led to population influx, environmental deterioration, urban fragmentation, haphazard landscape development, stress on ecosystem structure, and alteration of land use patterns (Thapa, 2009). According to UNHABITAT (2015), Kathmandu is vulnerable to the impact of climate change. So this research aims to investigate the impact of urban growth on land surface temperature in the valley, since LST is an important factor controlling urban climate. Moreover, quantifying LULC change is also essential for monitoring spatial-temporal processes of urban growth and its environmental consequences in the valley.

Research related to the relationship between LULC change and LST, or UHI effect in the Kathmandu valley has been limited so far. Even though climate change has been a hot topic, it seems like impact of urban sprawl on UHI effect has not been paid much attention. Thus the output of this research is assumed to fill this research gap through local scale analysis of landscape change detection and its influence on urban climate at a micro level. Our research will use surface temperature derived from airborne satellite image thermal band. On contrary to temperature data collected from weather stations, the satellite image data provides wide spatial coverage and is thus useful to reveal comprehensive spatial pattern of UHI at large scale more accurately. In our research, we determined LULC change over time, observed spatial-temporal pattern of urban growth through urban fragmentation, conducted hot

spot analysis to see the UHI formation and explored the relationship between LULC change and UHI effect comprehensively.

This research presents a detailed study on the impact of urban growth on land surface temperature in the Kathmandu valley. It provides evidence on the alteration of land use and land cover due to urban growth and the existence of UHI phenomenon in the valley. Exploring the impact of urban growth on LST can be useful for the urban planners and decision makers for sustainable urban planning and to discover ways to solve the urban problems. Moreover the outcome of this research will play a prominent role in promoting awareness of not only the concerned authorities but also to the urban residents. This will encourage them to foster effective urban management and contribute to improve urban environment. Concerned authorities can enforce effective plans and policies regarding land use and urban management while general public can develop community resilience to UHI effect by taking initiatives even from their home like installing green roofs and increasing greenery in their premises.

1.2 Aim & Objectives

Aim

The aim of this research is to analyze the impact of urban expansion on land surface temperature for the three year periods: 1988, 2000 and 2014, using GIS and Remote Sensing techniques on Landsat imagery.

Objectives

- To use supervised maximum likelihood classification to determine the spatial pattern of land use land cover change and analyze the dynamics of urban land use transformation in the study area for the given time period.
- To quantify change of each land cover class and determine the rate and spatial trend of urban growth.

- To determine land surface temperature change on each land use land cover type and investigate the relationship between surface temperature and land use land cover characteristics.
- To determine the appropriate approach between land use indices and land use land cover class for the future prediction of land surface temperature pattern in the study area based on non-parametric regression.

1.3 Research Questions

- During the study period what changes have occurred in the LULC types?
- How is the trend of urban growth in the study area?
- How is the spatial pattern of land surface temperature in the study area?
- What is the relationship between the land surface temperature and land surface characteristics?
- Is there formation of Urban Heat Island in the study area? If so, how is its spatial-temporal pattern?

1.4 Research Structure

Figure 1 shows the brief structure of the thesis and the interconnection between its different chapters. Chapter 1 presents the background and motivation of the research, objectives and the research questions. Chapter 2 briefly describes about the data, software and the study area. Chapter 3 discusses on the detailed methodology used in this research. Chapter 4 presents the results and its discussions. Finally, Chapter 5 concludes the research with the achievements, limitations of the research and the future works.

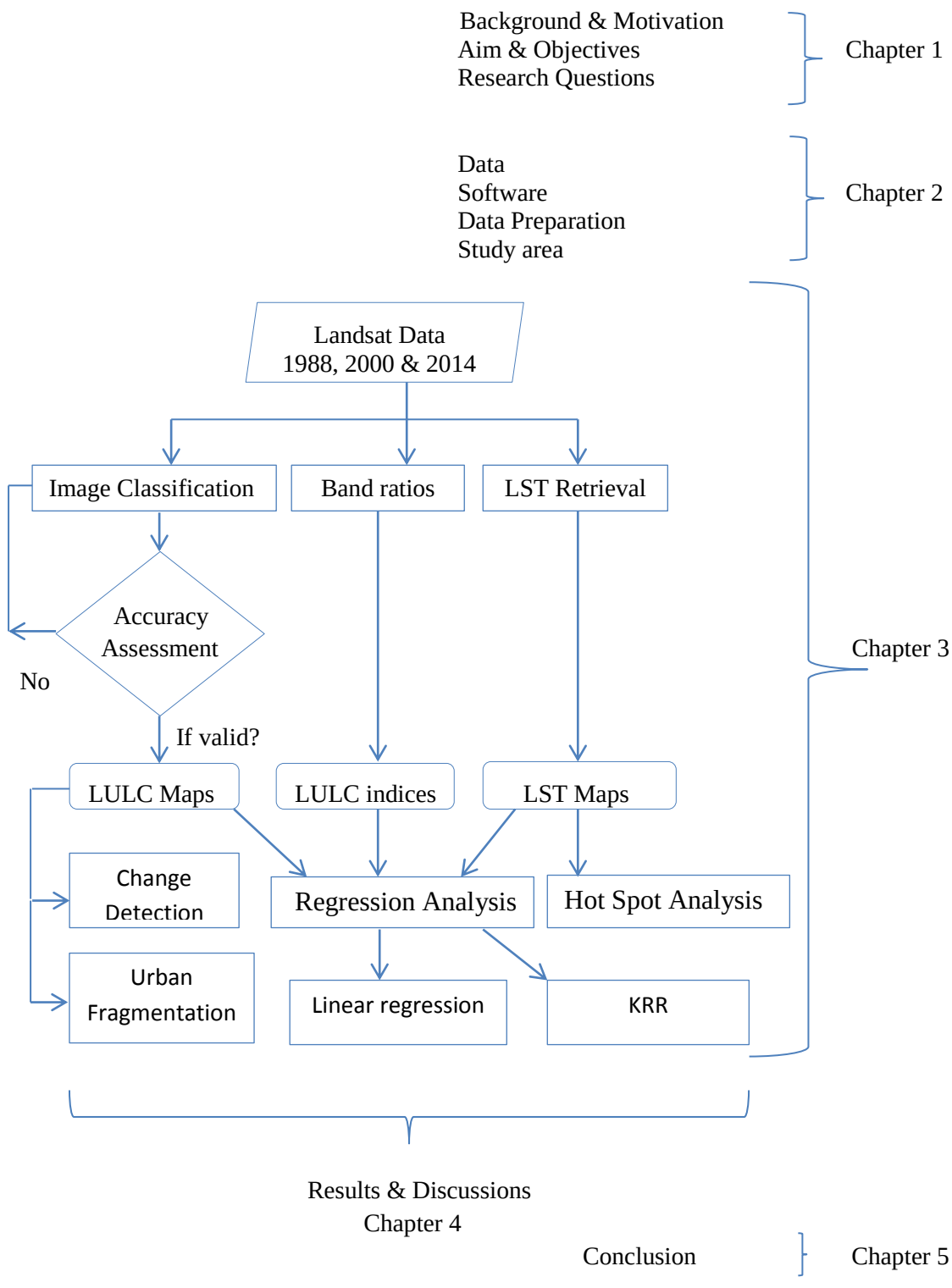

Figure 1: Structure of the thesis

2. DATA & STUDY AREA

2.1 Data

Primary data used for this research include Landsat satellite imagery: Landsat 5 Thematic Mapper (TM) and Landsat 8 Operational Land Imager (OLI), acquired on April 3, 1988; April 4, 2000; and April 11, 2014. These Landsat data can be freely accessed from the USGS portal, and is processed by NASA to generate radiometric calibration and atmospheric correction algorithms to the Level-1 products (http://earthexplorer.usgs.gov/). To ensure better comparison of surface temperature and UHI effect we used satellite images from the month of April for all three years, which lies in the summer season. Further detail about the Landsat imagery has been tabulated below, while their band designations are given in appendices section.

Table 1: Detail Characteristics of images

S.N.	Satellite	Sensor	Bands (no.)	Imagery Date	Resolution (meter)	Path/Row
1	Landsat 5	TM	7	1988-04-03	30	141/041
2	Landsat 5	TM	7	2000-04-04	30	141/041
3	Landsat 8	OLI_TIRS	11	2014-04-11	30	141/41

Landsat images are amongst widely used satellite remote sensing data and their spatial, spectral and temporal resolution made them useful for mapping and planning projects (Landsat 7, 2011). Landsat images were used to classify land use land cover classes, retrieve LST and calculate NDVI, NDBI and NDWI indices. Besides Landsat images, the secondary data used in this research were high resolution IKONOS images, digital Orthophotos, digital topographic maps and different layers of Kathmandu valley such as road networks, water bodies and designated areas prepared by the Department of Survey, Nepal. The secondary data also included reports, statistical data and geographical information from various organizations of Nepal like DHM. These ancillary data were mostly used in classification and its accuracy assessment.

2.2 Software

Various software tools were used for the image processing, spatial analysis and map creation. They are as follows:

- ArcGIS 10.3.1
- Geomatica 2016
- R software
- MATLAB
- MS Office packages (Word & Excel)

Most of the spatial analyses such as change detection, urban fragmentation, determination of LST, hot spot analysis, were conducted using ArcGIS, while Geomatica was specifically used for the data preparation – atmospheric correction of the Landsat images, and digital image classification. Linear regression was performed with R software whereas Kernel Ridge Regression was performed using MATLAB. Besides, MS Office packages (Word, Excel) were used for documentation, tabulation and graphical representation of the results.

2.3 Data Preparation

In general, raw digital images contain distortions due to variations in altitude, earth curvature and atmospheric refraction (Kaiser et al. 2008). However, Level-1 Landsat standard products, used in this study are free of distortions from the aforementioned sources (http://earthexplorer.usgs.gov/). Nevertheless, as the acquired images contained negligible amount of haze, they were subjected to haze removal within the Atmospheric correction procedure. The spatial reference system for all the datasets was WGS 1984, UTM zone 45 N. Therefore, data which were not in this system – especially digital topographic maps and other layers of Kathmandu valley, were projected to that system. Digital Orthophotos were rectified using IKONOS image with WGS 1984, UTM zone 45 N using first order polynomial (Affine) transformation method. A total number of 20 GCPs were used to register the Orthophotos. In this way digital Orthophotos were georeferenced using an image to

image registration technique, which allowed Orthophotos to be used for direct comparison of features with Landsat images while collecting training samples for image classification and accuracy assessment. Finally, Landsat images were clipped to obtain the area of interest.

2.4 Study area

The study area is the Kathmandu valley of Nepal with an area of approximately 42356 hectares. Kathmandu valley is made up of Kathmandu, Lalitpur and Bhaktapur districts. The valley is bowl shaped and is situated between 27^0 32' 13" to 27^0 49' 10" N latitude and 85^0 11' 31" to 85^0 31' 38" E longitude. The average elevation is 1300 meters above mean sea level (Pant & Dongol, 2009). It is surrounded by four high hills: Shivapuri in the NW, Chandragiri in the SW, Nagarjun in the NE and Phulchoki in the SE. Their altitude ranges from 1500 m. to 2800 m. (Baniya, 2008). The major rivers flowing through the valley are *Bagmati*, *Bishnumati* and *Manohara*.

Kathmandu valley is the most developed and populated place in Nepal. Majority of the government offices, headquarters and commercial centers are located in the valley, making it the economic hub of the country. The valley is historically important as well, as it owns seven World Heritage Sites (Tourism portal, 2017). With an area of less than one percent of the country's total area only, Kathmandu valley accommodates 31% of the total urban population of the country (CBS portal, 2017). Urban growth in the valley accelerated since 1980s, and the growth rate was substantially high during the 1990 decade (Sharma, 2003).

As stated earlier, the valley is bordered by high hills and mountain ranges. They are composed of schist, gneiss and granitic rock in the North and slightly metamorphosed sedimentary rocks in the south, east and west. Different types of soil are found in the valley. Lacustrine soil is common in the lowlands, as geologists believe that Kathmandu valley was a big lake in the ancient time, while sandy soil and red soil are prevalent in the high hills. Mixed type of vegetation is found in the

valley with temperate, Pine and broad leaved forest being the major ones. The common species are *Pinus roxburghii, Alnus castonopsis, Schima wallichi, Ulnus nepalensis* (Adhikary, 2015; Katuwal, 2016; Piya, 2004; Shrestha, 1998).

The climate of Kathmandu valley is sub-tropical cool temperate. Maximum temperature is 35.6^0C in April and minimum is -3^0C in January. In general, temperature is 19^0C to 27^0C during summer and 2^0C to 20^0C during winter. The climate is influenced by tropical monsoon of southeast and receives average rainfall of 1400 mm. during June to August. There are three main seasons: winter lies in the month of November to February; summer lies in the month of March to May; and rainy season during June to October (Pant & Dongol, 2009).

Figure 2 shows the 3D perspective of the study area which is created by overlaying Landsat image over DEM in ArcScene. Figure 3 shows the location map of the study area.

Figure 2: 3D perspective of the study area

Figure 3: Location map of the study area

3. RESEARCH METHODS

This section deals with the various approaches applied to fulfill the aforementioned aim and objectives. These approaches illustrate the practical implications of GIS and Remote Sensing in relation to the use of spatial-temporal datasets to address real world problems, the UHI phenomenon in our case. The major methods used in our research are supervised maximum likelihood classification, change detection analysis, urban fragmentation, hot spot analysis and regression analysis.

3.1 Supervised Maximum Likelihood Classification

Supervised Maximum Likelihood Classification was used to classify the study area into land use land cover classes. In this method, the spectral characteristics of the classes were defined by identifying training samples. Knowledge about the area of interest played a vital role in this process. After the collection of training samples, image classification was carried out by applying the Maximum Likelihood Classification algorithm. The algorithm assigns a cell to the class of the highest probability, whereby the probability value is the statistical distance based on the mean values and covariance matrix of the clusters (Tempfli, 2009).

At least 50 pixels in an average were taken from spectrally enhanced images for each class as training samples. Color composites based on band combinations - 5, 4, 3 in Landsat 8 and 4, 3, 2 in Landsat 5 TM were created to enhance image interpretation. Likewise high resolution IKONOS images, digital Orthophotos and digital topographic maps were also used as reference. The classification result included six land use land cover classes: Urban, Agriculture, Forest, Bare soil, Open area and Water. These classes were in accordance to the existing practices in the Kathmandu valley as well as the system adopted by the Survey Department of Nepal. Urban area covered built up areas comprising buildings, roads, airport runway and other impervious surfaces. Agriculture represents cropland while bare soil means clear exposed surfaces such as preconstruction areas, river banks not covered by the vegetation etc. Lands with little vegetation cover were classified as Open area. In this

way the final land use land cover maps were produced for all three years 1988, 2000 and 2014 respectively. These maps enabled spatial-temporal change analysis.

3.2 Accuracy Assessment

Usually LULC maps derived from classification contain some errors due to several factors that range from the initial data acquisition procedure to the implementation of the classification technique. Thus accuracy assessment of classification results is mandatory. The most common method generally used for the accuracy assessment is the error matrix (confusion matrix). An error matrix is an arrangement of numbers representing number of samples assigned to a specific category relative to the ground truth, in rows and columns. The rows in the matrix represents classification derived LULC maps while columns represent reference data collected from the field work. This matrix enables computation of several statistical measures such as overall classification accuracy, error of omission and commission, and kappa coefficient (Congalton and Green, 1999).

Overall accuracy is defined as the ratio of the number of correctly classified pixels (i.e. the sum of the diagonal elements) to the total number of pixels checked, expressed in percentage. However, overall accuracy is an average, so it does not reveal how error is distributed between the classes. Therefore, other measures like error of omission and error of commission were introduced. Error of omission is the percentage of pixels that should have been put into a given category but were not. Error of commission is the percentage of pixels placed in a given category when they actually belong to the other category. Error of omission corresponds to Producer's accuracy and error of commission corresponds to User's accuracy. Thus Producer's accuracy represents the percentage of a given category correctly identified on the map and User's accuracy represents the probability that the given pixel will appear on the ground as it is categorized. The kappa statistics reflects the difference between actual agreement and the agreement expected by chance. It incorporates the off diagonal elements of the error matrix (Foody, 2002; Lillesand et al., 2007; Tempfli, 2009).

The Kappa coefficient was calculated according to the equation (1) given by Congalton and Green (1999):

$$K = \frac{N\sum_{i=1}^{r} X_{ii} - \sum_{i=1}^{r}(X_{i+} \times X_{+i})}{N^2 - \sum_{i=1}^{r}(X_{i+} \times X_{+i})} \quad (1)$$

where,

r = no. of rows in the error matrix

X_{ii} = no. of observations in row i column i (along the diagonal)

X_{i+} = marginal total of row i (right of the matrix)

X_{+i} = marginal total of column i (bottom of the matrix)

N = total no. of observations in the matrix

For the accuracy assessment of our classification results, 250 random points were taken from the classified image to compare with high resolution IKONOS images and digital Orthophotos. Based on this, we calculated the Overall accuracy, User's accuracy, Producer's accuracy and Kappa index to evaluate the classification accuracy.

3.3 Land Surface Temperature Retrieval

Land surface temperature was retrieved from the thermal infrared band of Landsat images (band 6 of Landsat TM 5 and band 10 of Landsat 8). The basic steps for the retrieval of LST given below are based on the guidelines provided in Landsat Data Users Handbook published by USGS (Landsat 7, 2011; Landsat 8, 2015). Besides, one of the methods discussed in the research article by Giannini et al. (2015) has been also taken as reference.

i. Conversion of pixel values to radiance

The pixel values from digital number units were converted into radiance using the header files parameters of Landsat images as follows:

For Landsat TM 5:

L_λ = Grescale * QCAL + Brescale (2)

which can be also expressed as:

$$L_\lambda = \frac{(LMAX\lambda - LMIN\lambda)}{(QCALMAX - QCALMIN)} * (QCAL - QCALMIN) + LMIN\lambda$$

For Landsat 8:

L_λ = ML* QCAL + AL (3)

ii. Atmospheric correction

Removal of atmospheric effects from the thermal bands is essential to convert radiance to reflectance measures. Therefore, a specific atmospheric correction model called DOS-1 has been considered in this study. DOS-1 is applicable to multispectral image data only, and is explicitly an image based procedure, which means it does not require in situ measurements. DOS-1 model corrects for both atmospheric additive scattering component, attributed to path radiance and solar effects - solar irradiance and solar zenith (Chavez, 1996).

iii. Conversion of spectral radiance to at-sensor brightness temperature

$$T_B = \frac{K_2}{\ln(\frac{K_1}{L_\lambda} + 1)} \quad (4)$$

iv. Determination of emissivity

The correct determination of surface temperature is constrained to an accurate knowledge of surface emissivity. The emissivity of a surface can be determined as the contribution of the different components that belong to the pixels according to their proportions (Synder et al., 1998). In this study we used NDVI threshold method to determine emissivity as proposed by Sobrino, Jiménez-Muñoz & Paolini (Sobrino et al., 2004).

However, NDVI is calculated from the reflectance values of the visible and near infrared bands as follows:

$$\text{NDVI} = \frac{(\rho_{NIR} - \rho_{RED})}{(\rho_{NIR} + \rho_{RED})} \quad (5)$$

where, ρ_{NIR} and ρ_{RED} are the reflectance obtained by applying the DOS-1 method as mentioned above, at the Near Infrared band and Red band, for atmospheric effect correction.

v. Land Surface Temperature retrieval

The land surface temperature corrected for spectral emissivity is computed as follows (Artis & Carnahan, 1982):

$$\text{LST} = \frac{T_B}{\left(1 + \left(\lambda \frac{T_B}{\rho}\right) * ln \in\right)} \quad (6)$$

where,

λ is the central band wavelength of emitted radiance (11.45 μm)

ρ = h * c/ σ ($1.438*10^{-2}$m*K) with: h is the Planck's constant ($6.62* \ 10^{-34}$J*s),

c is the velocity of the light ($2.998*10^{8}$ m/s) and

σ is the Boltzmann constant (1.38*10-23 J/K)

vi. Convert land surface temperature value from Kelvin unit to degree Celsius

$$\text{LST } (^{0}\text{Celsius}) = \text{LST (Kelvin)} - 273.15 \quad (7)$$

Table 2 below defines all the parameters introduced above.

Table 2: Parameters in LST Retrieval

Parameters	Definition
L_λ	the spectral radiance at the sensor's aperture
Grescale	the rescaled gain (the data product "gain" contained in the Level 1 product header or ancillary data record)
Brescale	the rescaled bias (the data product "offset" contained in the Level 1 product header or ancillary data record)
QCAL	the quantized calibrated pixel value
LMINλ	the spectral radiance that is scaled to QCALMIN
LMAXλ	the spectral radiance that is scaled to QCALMAX
QCALMIN	the minimum quantized calibrated pixel value (corresponding to LMINλ)
QCALMAX	the maximum quantized calibrated pixel value (corresponding to LMAX λ)
ML	the radiance multiplicative scaling factor for the band (*RADIANCE_MULT_BAND_n* from the metadata)
AL	the radiance additive scaling factor for the band (*RADIANCE_ADD_BAND_n* from the metadata)
K_1, K_2	the calibration constants
ϵ	the emissivity of the surface

3.4 Land use Land Cover Indices

NDVI (Normalized Difference Vegetation Index), NDBI (Normalized Difference Built-up Index) and NDWI (Normalized Difference Water Index) indices were used to determine the relationship between LULC and LST. These indices can be useful to assess and monitor the urban thermal environment. Some of these indices were even used to delineate LULC types based on the appropriate threshold values. Besides LULC indices, DEM was also used in the analysis. DEM of the study area was generated based on the contour lines available at 20 meters interval and spot heights.

LULC indices were extracted from the satellite images based on the following expressions:

$$NDVI = (NIR - R) / (NIR + R) \quad \text{(Rouse et al., 1974)} \quad (8)$$

$$NDBI = (MIR - NIR) / (MIR + NIR) \quad \text{(Zha et al., 2003)} \quad (9)$$

$$NDWI = (G - MIR) / (G + MIR) \quad \text{(Xu, 2006)} \quad (10)$$

where, G, R, NIR, MIR are Green, Red, Near Infrared and Mid – infrared bands respectively.

3.5 Regression Analysis

3.5.1 Linear Regression

We applied multiple linear regression analysis to determine the relationship between LST and LULC. A multiple linear regression analysis is the statistical process useful for estimating the relationships among multiple explanatory variables (independent variables) and a predictor (dependent variable). It is the generalization of linear regression to multiple variables which can be expressed as (Higgins, 2005):

$$Y_i = \beta_0 + \beta_1 X_{i1} + \beta_2 X_{i2} + \ldots\ldots\ldots + \beta_r X_{ir} + \epsilon_i \quad (11)$$

where, we consider n no. of observations of one predictor and r explanatory variables.

$Y_i = i^{th}$ observation of the predictor

$X_{ij} = i^{th}$ observation of the j^{th} explanatory variable (j = 1, 2, 3…, r)

β_j = parameters to be estimated

$\epsilon_i = i^{th}$ independent identically distributed normal error

We extracted LST and LULC indices – NDVI, NDBI, NDWI, and DEM for each pixel in the study area. Three thousand random points were obtained from the LST image and their corresponding LULC indices values were extracted in ArcGIS to use them in the linear regression model. Such model gives us a general idea about the relationship between LST and LULC. However we applied a non-linear regression method called Kernel Ridge Regression (KRR) to determine the predicted value of LST because this method is better and more flexible when many explanatory

variables are taken into account (Saunders et al., 1998). We used many LULC variables which may create non-linear correlations; therefore KRR would be suitable for our purpose.

3.5.2 Non-linear Regression

Ridge Regression technique is especially designed to deal with multi-collinearity or non-linear dependence of regressors (Rosipal & Trejo, 2001). It is a generalization of least square regression. For example, in case of linear regression, let us assume that the aim is to fit the linear function $y = \omega \cdot x$ to our training set $\{(x_1, y_1), \dots, (x_T, y_T)\}$ where T is the no. of examples, x_t is a vector in R^n (n is no. of attributes) and $y_t \in R$, t = 1,2,…,T. Least square recommends assessing $\omega = \omega_0$ which minimizes:

$$L_T(\omega) = \sum_{i=1}^{T} (y_i - \omega \cdot x_i)^2 \qquad (12)$$

and using ω_0 for labeling future examples: if a new example has attributes x then the predicted label will be $\omega_0\, x$.

Ridge regression slightly modifies this equation to:

$$L_T(\omega) = a\|\omega\|^2 + \sum_{i=1}^{T} (y_i - \omega \cdot x_i)^2 \qquad (13)$$

where, a is a fixed positive constant.

There are different ways to obtain the $\{(a, \omega)\}$ parameters. One of them is applying constrained minimization methods to the so-called "dual version" of equation (13). In this case, the estimation depends on the dot products of the x elements, i. e. $x_i \cdot x_j$.

KRR is a modification of equation (13) in such a way that non-linear functions can be fitted implicitly. In this case the aim is related to the estimation of a mapping function ϕ which "transforms" the training points to higher dimensional spaces $(x_i \to \phi(x_i))$ whereby we can deal with the problem as a linearization of the non-linear lower dimensional space where the x_i points lie. It can be shown that the dot products of the x elements, i.e., $x_i \cdot x_j$ are transformed into $\phi(x_i) \cdot \phi(x_j)$ which is known as "transformation kernel" (Saunders et al., 1998).

3.5.3 Experimental setup for the appropriate approach assessment for LST prediction

In order to determine the appropriate approach between LULC indices and LULC class for future LST prediction, first of all, we generated training sets for both LULC indices and LULC class. In case of LULC indices, we obtained training sets as we discussed previously for the linear regression method. But for the LULC class, initially we calculated the proportion of each land use land cover class using three different window sizes: 5 by 5, 10 by 10 and 20 by 20 which means 150 m, 300 m and 600 m pixel resolution respectively. Then we obtained their corresponding mean LST values. Zonal statistics tool was used to summarize the value of LST within each window. After that, we selected three thousand random samples from each of these three resolutions to generate the training sets for LULC class. Next, we trained KRR for both LULC class and LULC indices and then validated them on the corresponding test sets. As per our data, we used LST of 1988 and 2000, and LULC indices of 2014 to obtain the predicted values of LST in 2014. Similarly for LULC class, we used LST of 1988 and 2000, and LULC of 2014 for all 5*5, 10*10 and 20*20 window cases to obtain the predicted LST for 2014. Finally we computed RMSE between measured LST values and predicted LST values in 2014 for all the training sets of both LULC indices and LULC class to determine the suitable approach for LST prediction.

3.6 Hot Spot Analysis

Hot Spot Analysis tool in ArcGIS was used to identify statistically significant hot spots and cold spots from our LST datasets. This tool calculates the Getis-Ord Gi* statistic given a set of weighted features. Thus the LST raster datasets were converted to polygon features prior to analysis. The Getis-Ord Gi* Statistics is defined as:

$$G_i^* = \frac{\sum_{j=1}^{n} w_{i,j}x_j - \bar{X}\sum_{j=1}^{n} w_{i,j}}{s\sqrt{\frac{n\sum_{j=1}^{n} w_{i,j}^2 - \left(\sum_{j=1}^{n} w_{i,j}\right)^2}{n-1}}} \quad (14)$$

where, x_j is the attribute value for feature j, $w_{i,j}$ is the spatial weight between feature i and j, n is the equal to the total number of features and:

$$\overline{\mathrm{X}} = \frac{\sum_{j=1}^{n} x_j}{n} \quad (15)$$

$$\mathrm{S} = \sqrt{\frac{\sum_{j=1}^{n} x_j^2}{n} - \overline{\mathrm{X}}^2} \quad (16)$$

Note: The Gi* statistic is the z-score so no further calculations are required.

The resultant z-score tells whether the features with either high or low values cluster spatially. A feature with high value may not be statistically significant. To be statistically significant a feature should have a high value and be surrounded by other features with high values as well. Besides z-score the output feature class also contained p-value and confidence level bin (Gi_Bin). A high z-score and small p-value for a feature would indicate spatial clustering of high values. On the other hand, a low negative z-score and a small p-value would indicate spatial clustering of low values (ESRI, 2016). On the basis of Gi_Bin, we categorized LST classes as very hot spot, hot spot, warm spot, not significant, cool spot, cold spot and very cold spot.

3.7 Urban Fragmentation

As our research focuses on urban growth, the study of urban fragmentation is relevant. Urban fragmentation helps us to understand the urban landscape, so this research analyses the spatial-temporal dynamics of urban fragmentation in the study area. Fragmentation metrics proposed by Angel et al. (2012) have been used in our study. They are as follows:

Infill: It is a new development that has occurred between two time periods within the urbanized open space of the earlier period, excluding exterior open space;

Extension: A kind of development between two time periods in contiguous clusters that contained exterior open space in the earlier period and that were not infill;

Leapfrog: All new construction that occurred between two time periods in the open countryside, entirely outside of the exterior open space of the earlier period;

The terminologies introduced in the above metrics are defined as follows:

Fringe open space: It consists of all pixels within 100 meters of urban and sub urban pixels;

Captured open space: It consists of all open space clusters that are fully surrounded by built up and fringe open space pixels and are less than 200 hectares in area;

Exterior open space: It consists of all fringe open space pixels that are less than 100 meters from the open countryside;

Urbanized open space: It consists of all fringe open space, captured open space and exterior open space pixels in the city;

Urban built-up pixels: Pixels which have more than 50 percent of built-up pixels within their walking distance circle;

Suburban built-up pixels: Pixels which have 10-50 percent of built-up pixels within their walking distance circle;

Rural built-up pixels: Pixels which have less than 10 percent of built-up pixels within their walking distance circle;

Walking distance circle: It is a circle with an area of 1 km^2 around a given built-up pixel.

We applied Urban Landscape Analysis tool, developed by CLEAR, University of Connecticut (http://clear.uconn.edu/tools/ugat/index.html) to determine the spatial-temporal dynamics of urban fragmentation. The tool classifies urban area into Urban built-up, Suburban built-up, Rural built-up, Urbanized open land, Captured open land and Rural open land, based on spatial density of built-up area. In addition, the tool also classifies the new development, which has occurred between two consecutive time periods, as infill, extension and leapfrog, based upon its proximity to the previously existing development.

4. RESULTS & DISCUSSION

4.1 Land use land cover change in the study area

Table 3 summarizes the overall accuracy, user's accuracy, producer's accuracy and kappa coefficient of LULC classification accuracy assessment for the years 1988, 2000 and 2014.

Table 3: Accuracy Assessment of classified images for different years

	1988		2000		2014	
LULC types	User Ac.	Pro Ac.	User Ac.	Pro Ac.	User Ac.	Pro Ac.
Urban	86.11	83.78	93.10	81.81	90.00	87.50
Agriculture	87.23	87.23	89.09	87.50	76.60	82.00
Forest	91.22	89.65	92.10	94.59	91.66	91.66
Open area	76.59	83.72	87.87	81.69	75.00	83.34
Bare soil	81.08	78.94	77.77	90.32	85.71	88.23
Water	92.30	88.88	80.76	95.45	95.00	88.36
Overall Ac.	85.60		87.20		88.00	
Kappa stat.	0.82		0.84		0.85	

Note: User Ac. = User's Accuracy Pro. Ac. = Producer's Accuracy
Overall Ac. = Overall Accuracy Kappa stat. = Kappa Coefficient

Therefore, the overall accuracies for the years 1988, 2000 and 2014 were 85.60 %, 87.20 % and 88 % respectively. Forest and Water got the maximum accuracy in all three years. Meanwhile, Open area got the minimum accuracy. The kappa coefficients for the classification images were 0.82, 0.84 and 0.85 respectively.

Based on the supervised maximum likelihood classification technique as discussed in the methodology section, LULC maps were obtained for all three years and then area estimates and change statistics were computed. Figures 4-6 show the LULC maps for the year 1988, 2000 and 2014 respectively.

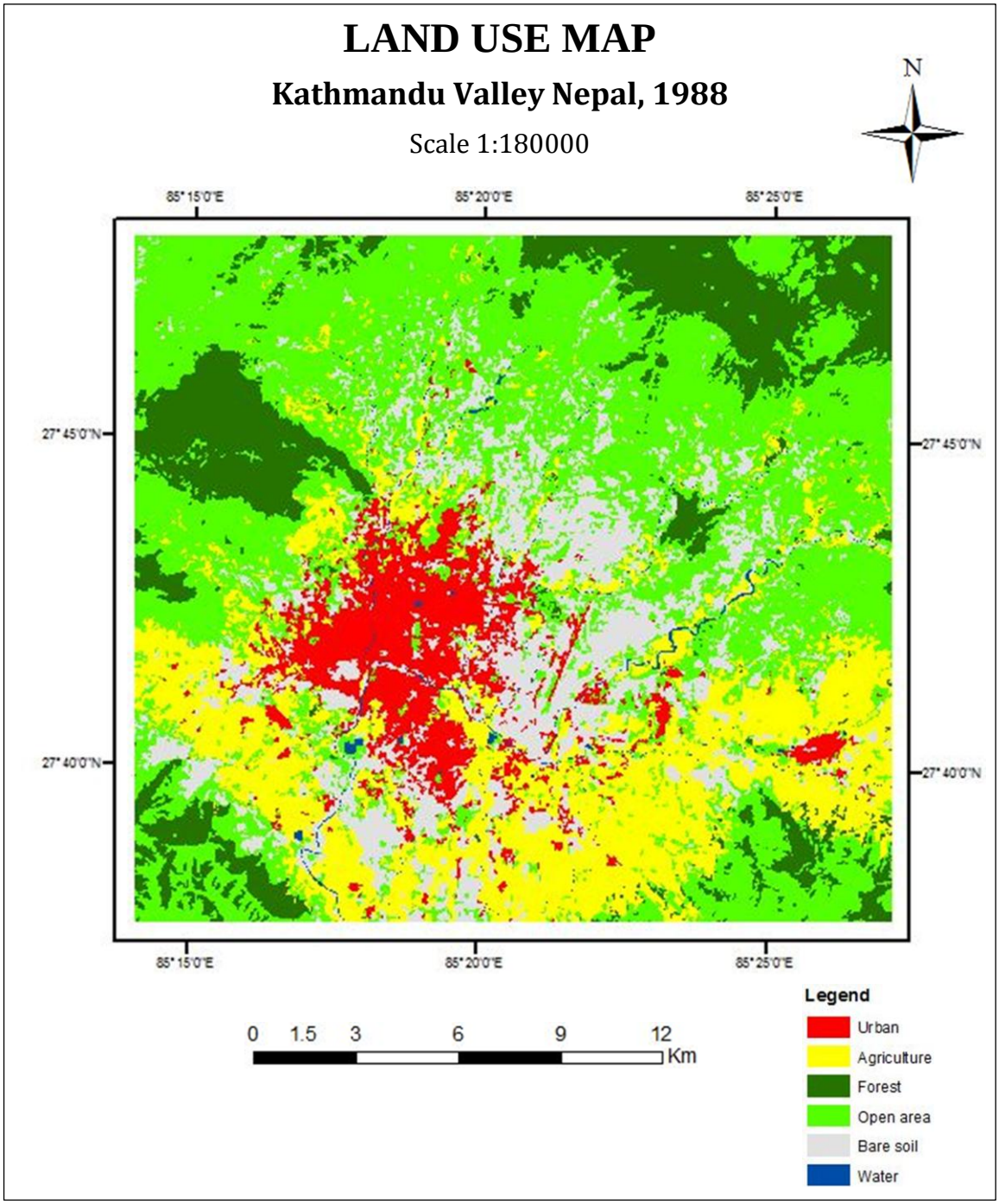

Figure 4: Land use land cover map of study area in 1988

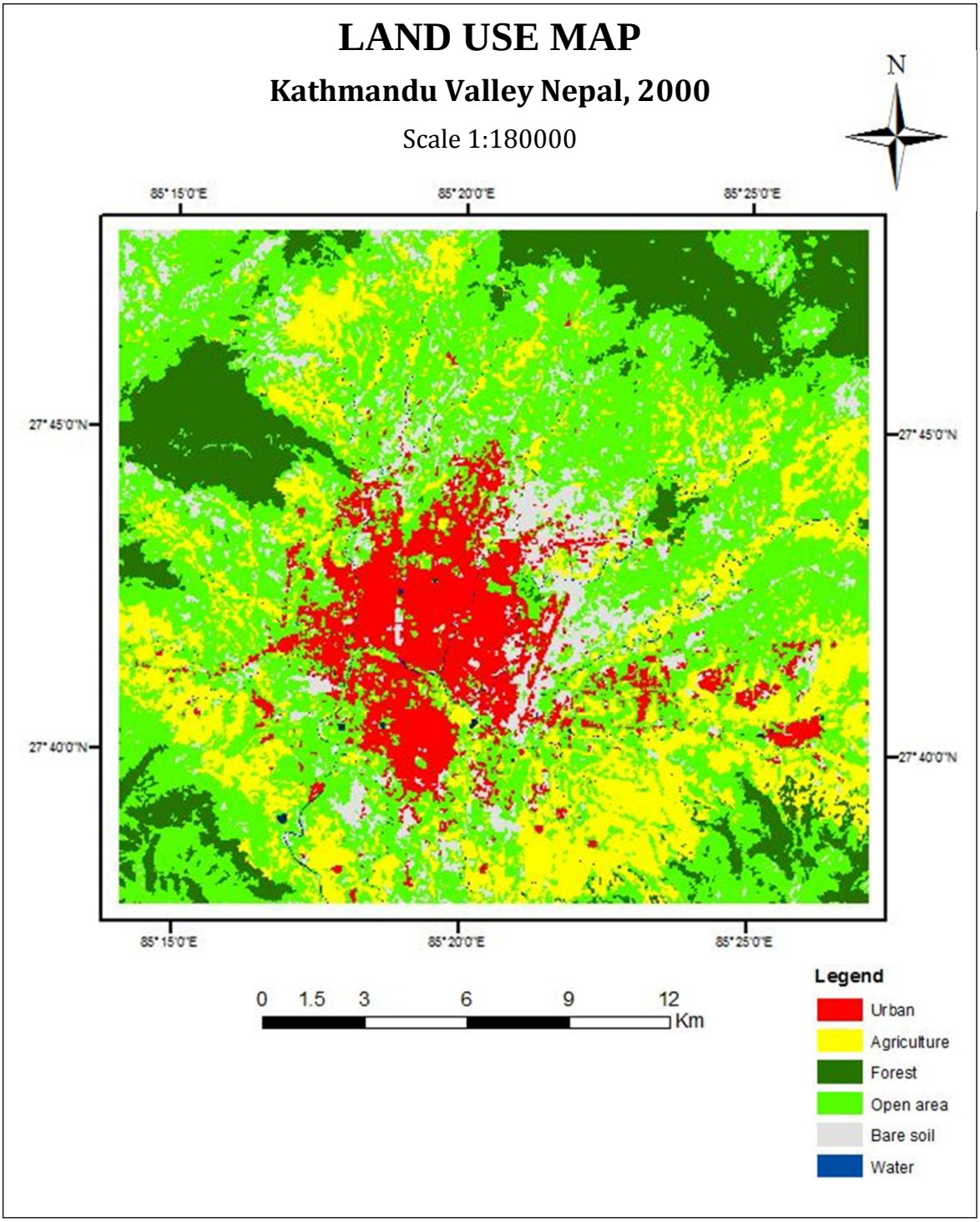

Figure 5: Land use land cover map of study area in 2000

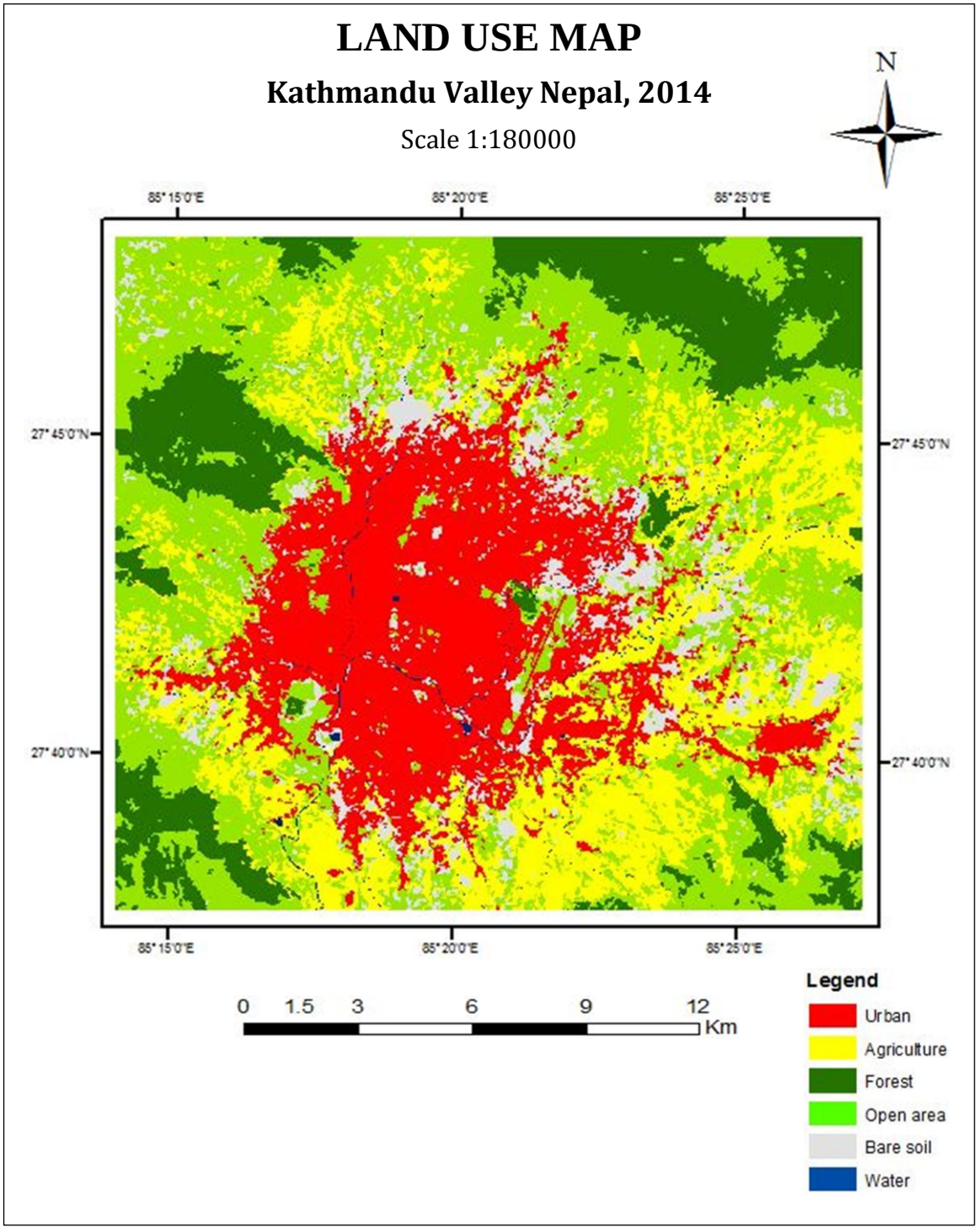

Figure 6: Land use land cover map of study area in 2014

Table 4 summarizes the area estimates for the land use land cover classes of the study area derived from the classification results. Among all LULC types, Open area constituted the predominant type of land cover in all three years occupying 42.59 percent of the total area in 1988, 45.25 in 2000 and 33.64 in 2014. Agriculture is the second largest land use type covering 19.85 percent of the total area in 1988, 19.72 in 2000 and 21.61 in 2014. Bare soil follows Agriculture accounting for 15.38 percent of the total area which is approximately 1 percent greater than that of Forest in 1988. However, Forest precedes Bare soil by almost two folds in the succeeding years. Water constitutes the lowest land cover, which is around 2 percent of the total area. Urban shows dramatic increase in area from 5.75 percent in 1988 to 20.63 percent in 2014.

Table 4: Area statistics of land use land cover classes for 1988 to 2014

LULC	1988		2000		2014	
	Area (ha)	%	Area (ha)	%	Area (ha)	%
Urban	2436.64	5.75	4207.63	9.93	8736.38	20.63
Agriculture	8406.26	19.85	8351.02	19.72	9154.87	21.61
Forest	6036.09	14.25	6049.84	14.28	6140.14	14.50
Open area	18040.71	42.59	19168.08	45.25	14249.17	33.64
Bare soil	6513.9	15.38	3731.98	8.81	3279.06	7.74
Water	922.16	2.18	847.21	2.00	796.14	1.88

Figure 7 is the graphical representation of area statistics of land use land cover classes presented in the Table 4 above. The graph demonstrates that Open area is the major LULC type. Water occupies the small proportion of the total area. There is a significant increase in the Urban while opposite trend can be seen for Bare soil and Open area. Water and Forest observed slight changes during the study period.

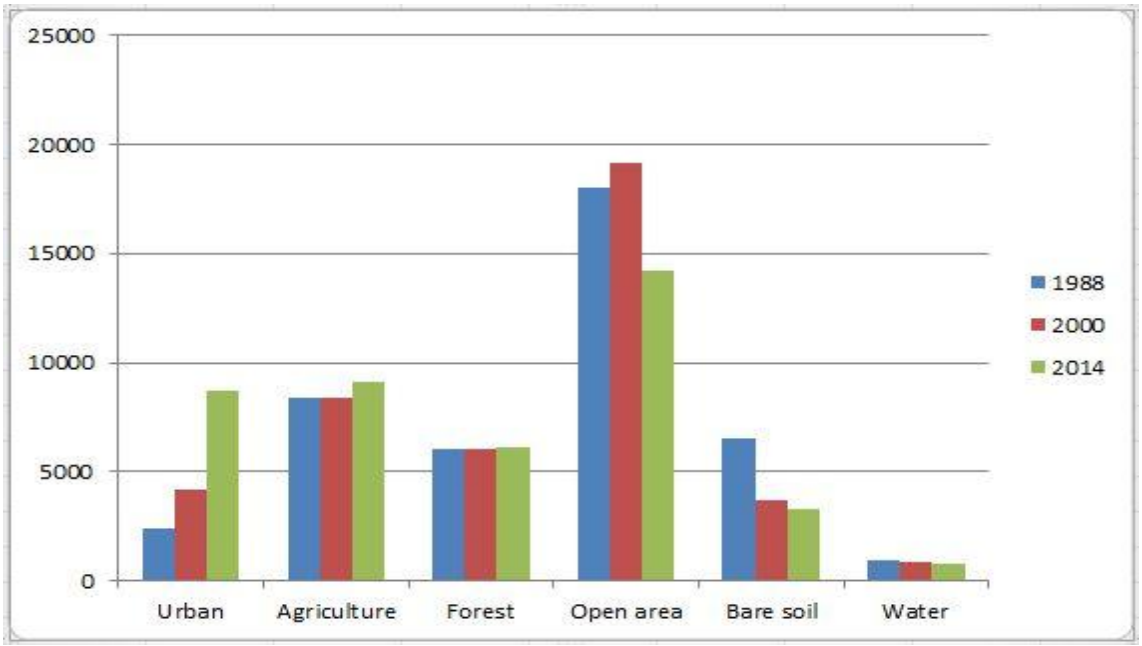

Figure 7: Land use land cover areas in different years

Likewise, Figures 8-10 and Table 5 illustrate the changes in all LULC types from 1988 to 2014. Table 5 shows the numerical change in area of all LULC types in terms of hectare and percentage with respect to that of corresponding LULC types in the previous year, whereas Figures 8-10 show the percentage change in area with respect to that of the given year graphically.

Table 5: Land use land cover change during 1988 - 2014

LULC	1988 – 2000		2000 - 2014		1988 – 2014	
	Area (ha)	%	Area (ha)	%	Area (ha)	%
Urban	1770.99	72.68	4528.75	107.63	6299.74	258.54
Agriculture	-55.24	-0.66	803.85	9.62	748.61	8.90
Forest	13.75	0.23	90.3	1.49	104.05	1.72
Open area	1127.37	6.25	-4918.91	-25.66	-3791.54	-21.02
Bare soil	-2781.92	-42.71	-452.92	-12.14	-3234.84	-49.66
Water	-74.95	-8.13	-51.07	-6.01	-126.02	-13.66

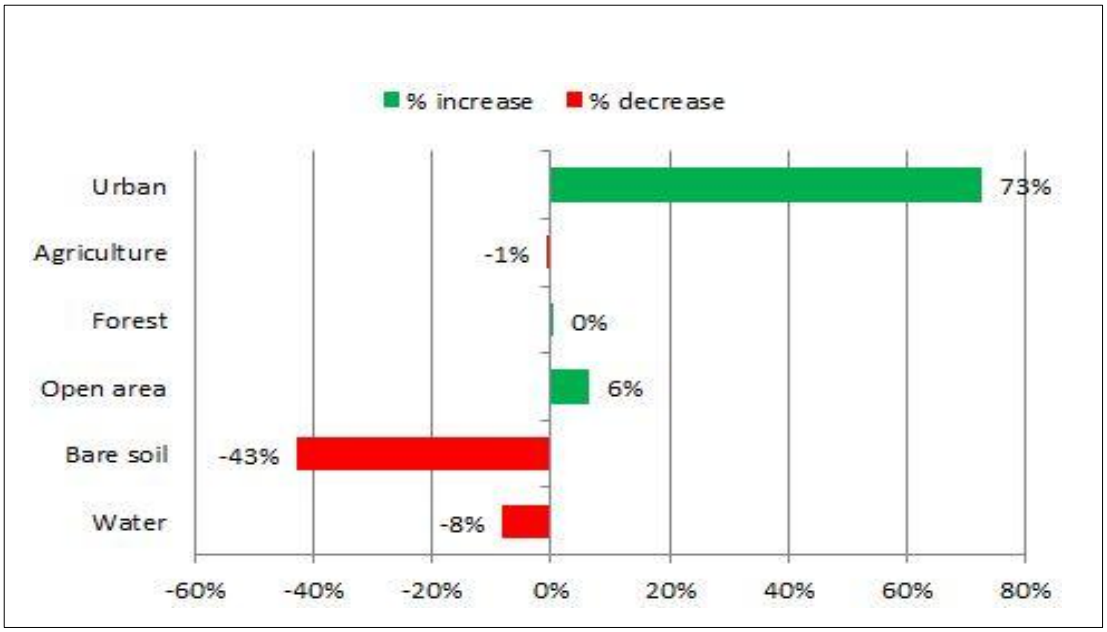

Figure 8: Percentage change in LULC between 1988 and 2000

During the first period (1988-2000) the land use change is characterized by abrupt rise in Urban area by approximately 73%. On the other hand Bare soil decreased by 43%. Open area increased by 6% whereas Water decreased by 8%. However there is no significant change in Forest and Agriculture.

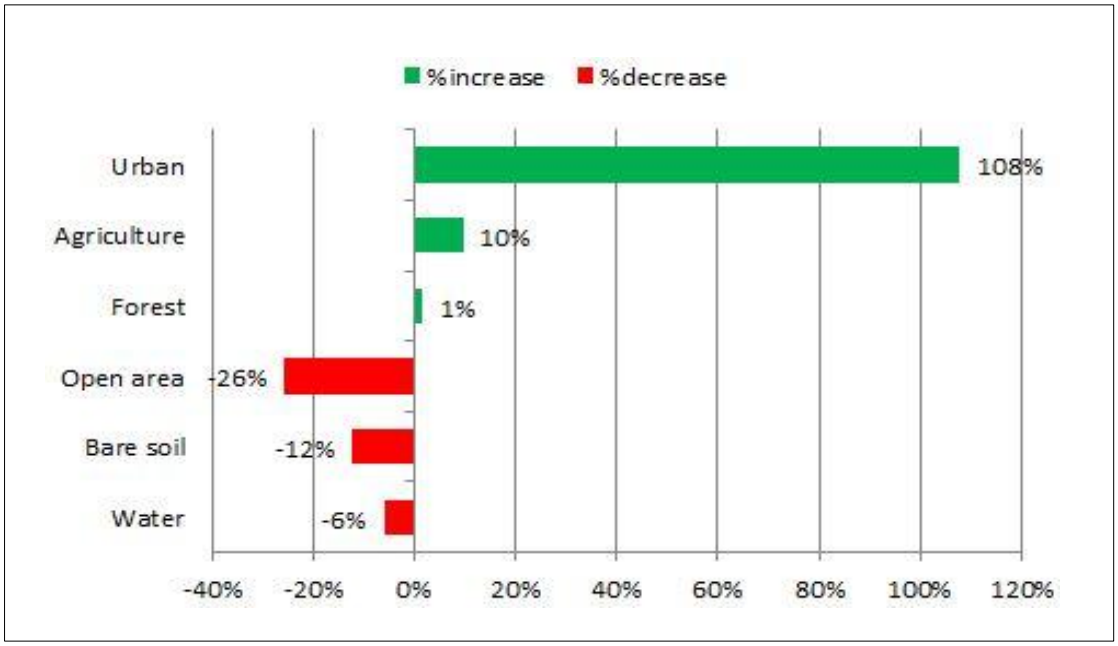

Figure 9: Percentage change in LULC between 2000 and 2014

In the second period (2000-2014), Urban increased sharply by approximately 108%. Open area showed an opposite trend in this period as compared to the first period with area declining by 26%. For Bare soil the declining trend reduced sharply from -43% to -12% in this period. Forest and Water maintained the same trend as that of the first period. Agriculture showed a sudden growth by 10%, though the changing trend was insignificant in the first period.

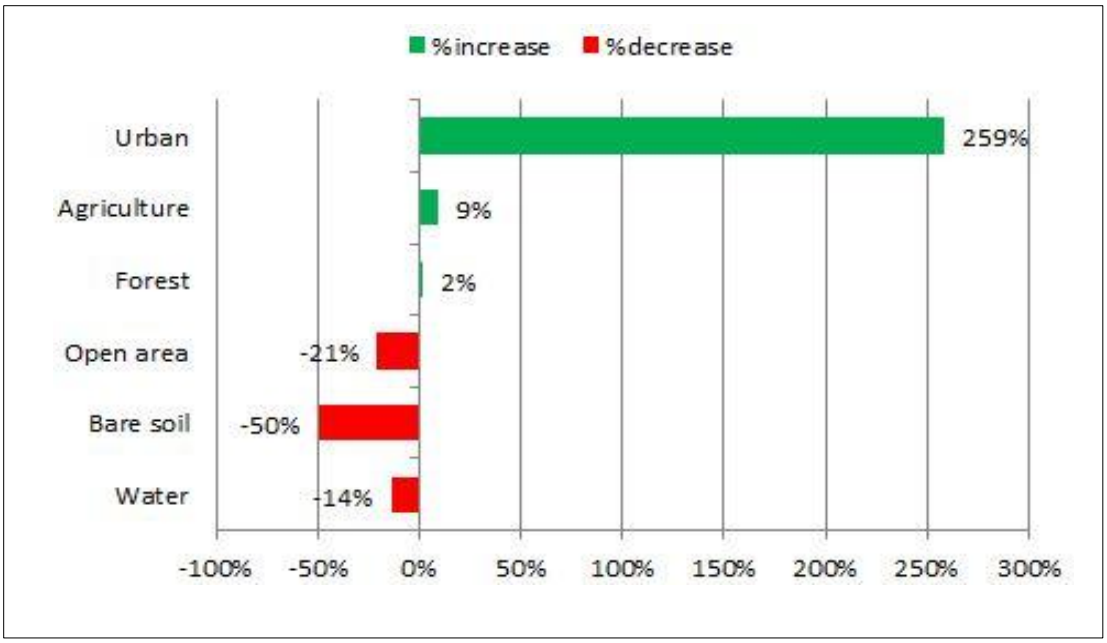

Figure 10: Percentage change in LULC between 1988 and 2014

This period (1988-2014) is in fact the overall change from the first and the second period. There is extreme increment in Urban land use by approximately 259% while Agriculture showed a nominal increment by 9%. Bare soil, Open area and Water were reduced by 50%, 21% and 14% respectively. Forest showed negligible increment of 2% over the period of 26 years.

Figure 11 demonstrates urban growth during different time periods: 1988 – 2000, 2000 – 2014 and 1988 – 2014. Urban growth has been categorized into three classes: infill, extension and leapfrog. From these maps, it can be clearly seen that extension type of growth was greater towards the north. This is due to the fact that lands on the

other directions especially to the west are comparitively less accessible, undulating and difficult to develop (Thapa, 2009). Table 6 summarizes the proportion of urban growth types during different periods. The table shows that extension type of growth was dominant in all periods, whereas infill and leapfrog types of growth were comparitively low.

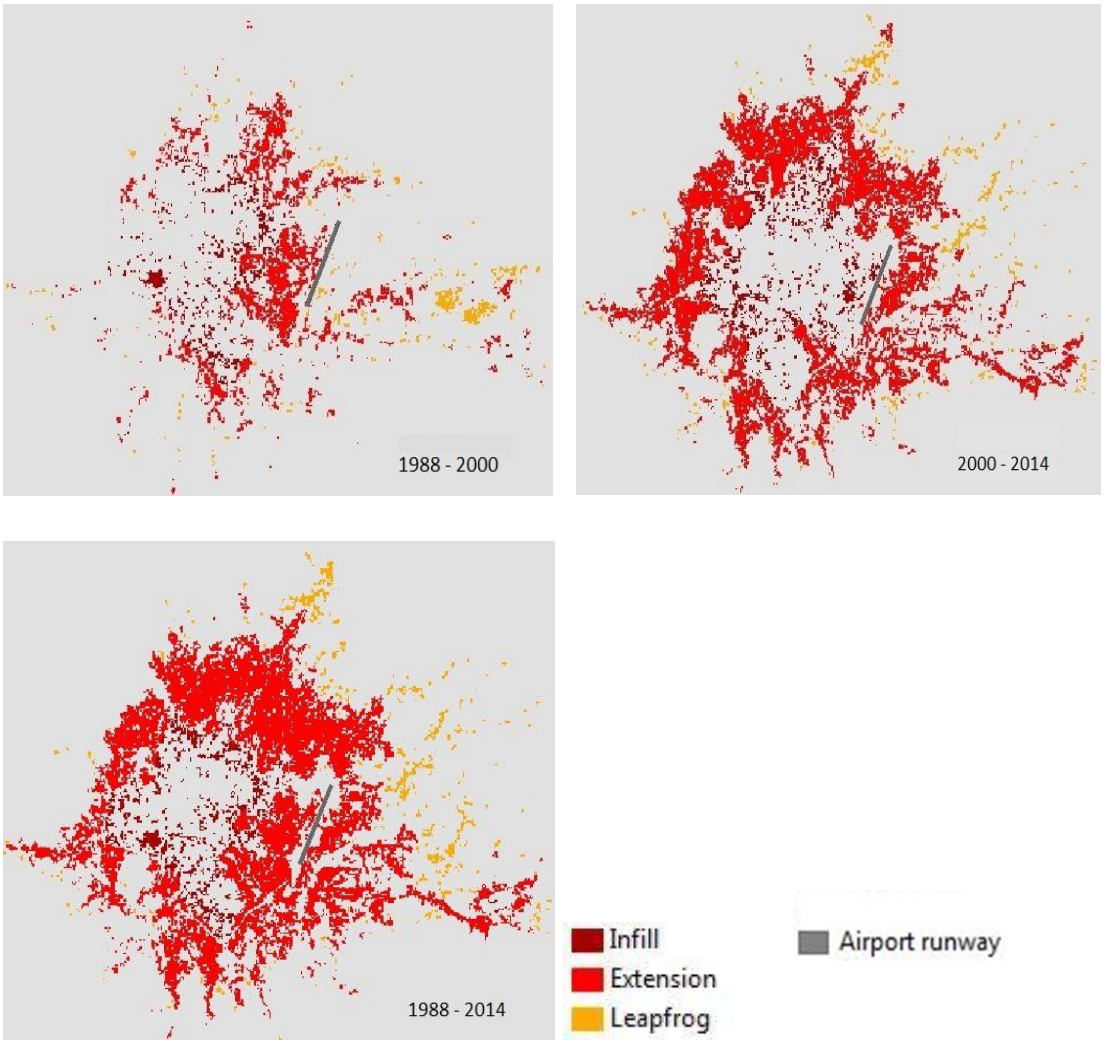

Figure 11: Urban growth types in different periods

Table 6: Proportion of various urban growth types in different periods (%)

	Different Periods		
Urban Growth type	**1988 - 2000**	**2000 - 2014**	**1988 – 2014**
Infill	18.32	10.85	8.72
Extension	67.90	82.22	84.19
Leapfrog	13.78	6.93	7.09

Apart from urban growth types, we also obtained urban landscape classes to analyze the impact of different levels of urbanization. Five classes: urban built-up, suburban built-up, rural built-up, urbanized open land and rural open land were mapped for urban landscape (Figure 12). Table 7 shows the proportion of urban landscape classes for different years. There is a gradual increment in urban built-up area at the expense of rural open land.

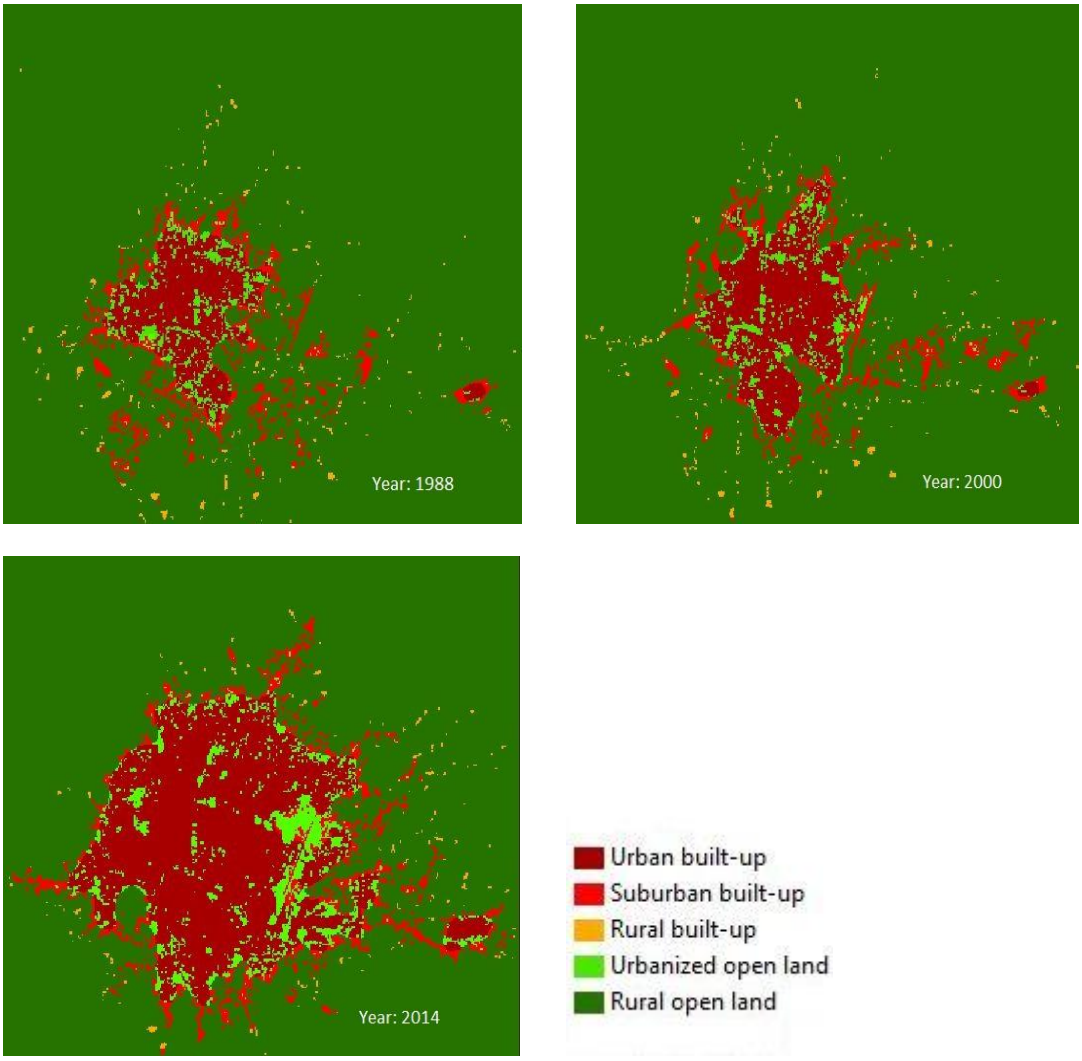

Figure 12: Urban landscape classes for different years

Table 7: Proportion of various urban landscape types in different years (%)

Urban landscape	1988	2000	2014
Urban built-up	4.50	6.55	18.16
Suburban built-up	2.91	2.82	4.02
Rural built-up	0.54	0.55	0.37
Urbanized open land	1.58	1.86	4.23
Rural open land	90.46	88.22	73.21

4.2 Spatial pattern of LST and LULC indices

4.2.1 Land Surface Temperature

Figure 13 shows the LST maps of the study area in 1988, 2000 and 2014. LST ranged from 13.96^{0}C to 36.77^{0}C in 1988, 15.84^{0}C to 39.17^{0}C in 2000 and 16^{0}C to 33.98^{0}C in 2014. The maximum temperature increased by around 3^{0}C during 1988 to 2000 and then declined sharply in the year 2014 by around 6^{0}C. However, there is a gradual increase in the minimum temperature in the subsequent years. The sudden fall in the maximum temperature during 2000 to 2014 can be reasonable, as some days of the year in the past can be hotter despite of the influence of urban warming phenomenon caused by urban growth over time. LST pattern analysis indicates low temperature represented by blue tone at the edges in all maps that stands for the forest area. High LST represented by a red patch in the middle represents the impervious surface of the airport and the red patches at the edges represent bare soil and even rocks in the high cliffs. The central yellow region represents the urban area. At meticulous observation of the pattern, gradual removal of blue tone in the middle and formation of uniform yellow tone can be seen, which gives the impression of the UHI formation.

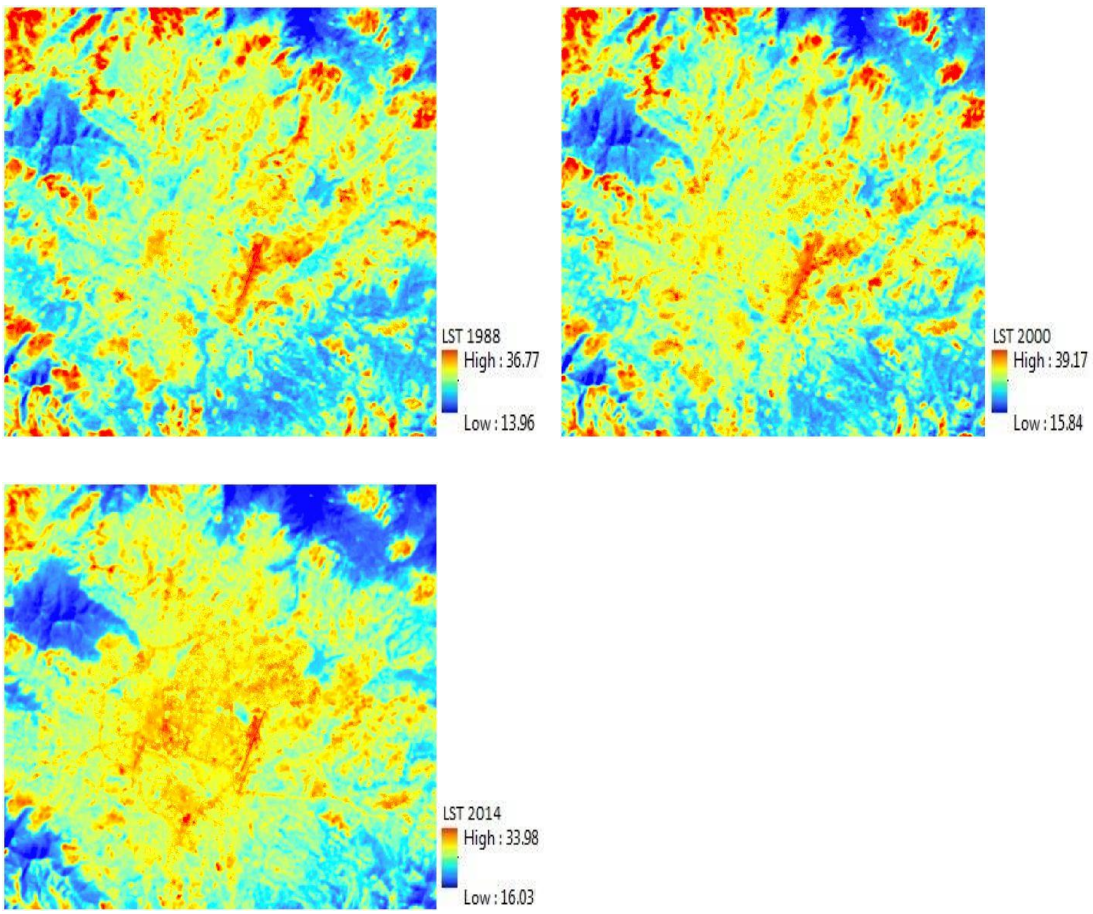

Figure 13: LST of the study area for the years 1988, 2000 and 2014

Figure 14 shows the mean LST within each LULC class in the study area. Forest LULC type got the minimum mean LST values in all three years (19.91^{0}C in 1988, 21.96 in 2000 and 20.58 in 2014) which is even lower than Water (21.52 in 1988, 23.99 in 2000 and 23.56 in 2014). Bare soil got the maximum mean LST values in all three years (29.10 in 1988, 30.84 in 2000 and 28.93 in 2014). After Bare soil, Urban area got the highest mean LST values (26.97 in 1988, 28.63 in 2000 and 28.08 in 2014). The mean LST for Open area is 25.16 in 1988, 27.59 in 2000 and 26.37 in 2014. Similarly the mean LST value for Agriculture is 22.93 in 1988, 26.83 in 2000 and 25.66 in 2014. In this way, Forest and Water received low mean LST values, Agriculture and Open area

received medium, and Bare soil and Urban received high values. The comparison of mean LST for Urban LULC type in the given years reveals that even though the maximum temperature in 2014 was lower than in 1988 and 2000, the mean LST value of Urban LULC type in 2014 is close to that of 2000 and much higher than in 1988. This justifies the urban warming effect in the study area due to urban growth over time.

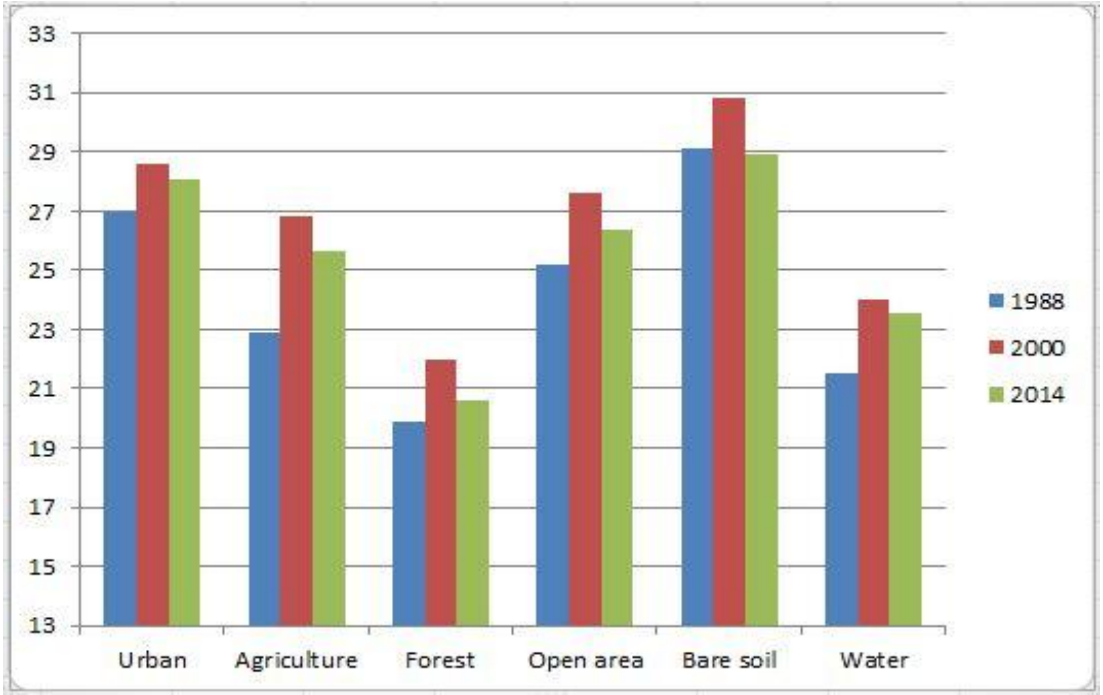

Figure 14: Mean LST for each LULC class in different years

4.2.2 Normalized Difference Vegetation Index

Figure 15 shows the spatial distribution of NDVI in the study area. The area with the highest NDVI values appeared in the edges, which represent the forest area. Low NDVI values can be observed concentrated primarily in the central region which corresponds to the urban area. The area with the lowest NDVI values were found in the ponds and rivers which are manifested as small dark red patches and thin curvilinear features respectively.

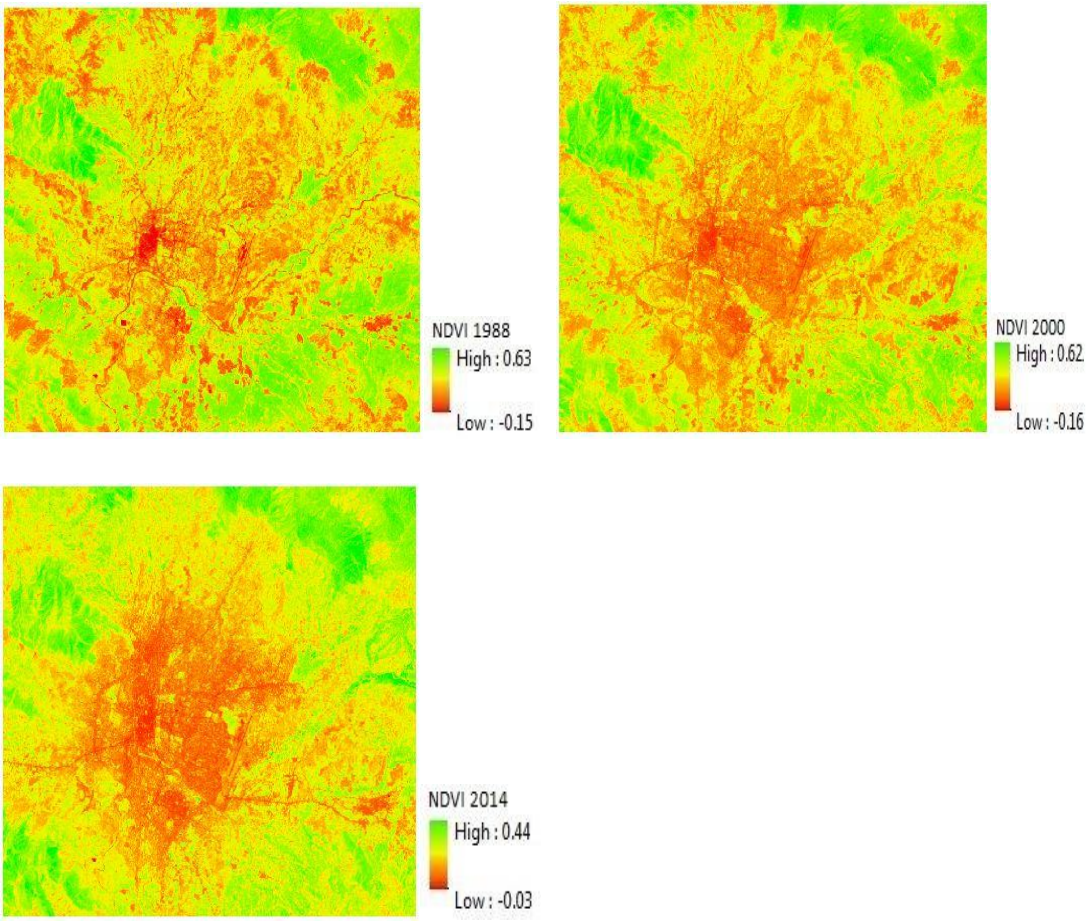

Figure 15: NDVI within each LULC class in 1988, 2000 and 2014

Figure 16 shows the bar chart of Mean NDVI values for each LULC class. The LULC class with the highest mean NDVI value is Forest with NDVI ranging from 0.45 to 0.30 for 1988 to 2014. The other LULC class with high NDVI value is Agriculture (0.24 to 0.37). Forest and Agriculture showed high NDVI values due to the dominance of vegetated cover. The lowest mean NDVI is for Water (-0.02 to 0.018) since water lacks vegetation. However it can be seen that its value tends to be positive over time and the possible reason might be due to the vegetation growth in water with increasing pollutants. NDVI value for the Open area is approximately around 0.2 while NDVI value for both urban and Bare soil is around 0.1.

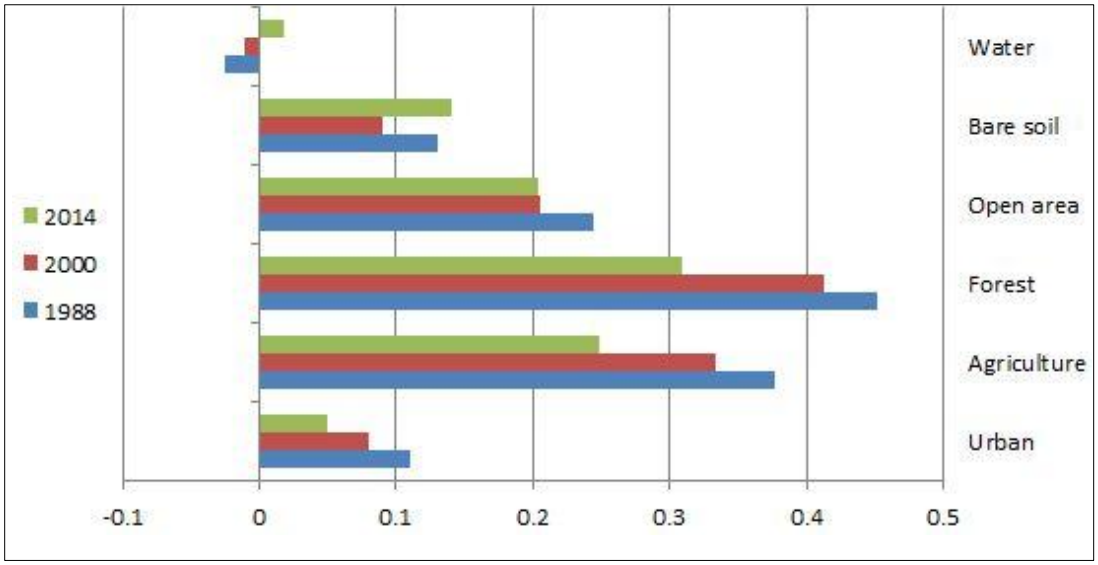

Figure 16: Mean NDVI values for each LULC class in 1988, 2000 and 2014

4.2.3 Normalized Difference Built-up Index

NDBI maps (Figure 17) revealed an opposite pattern to the NDVI maps in the sense that Forest, Agriculture and other vegetated areas with high NDVI values received low NDBI values. Likewise urban area with low NDVI received high NDBI value. The lowest NDBI is possessed by Water while the highest value is possessed by Bare soil. In general, built up areas have higher reflectance in relation to MIR band and is thus expected to have higher NDBI but some studies show that reflectance for certain types of vegetation increases as water content decreases (Cibula et al., 1992; Gao, 1996). The drier vegetation can even have higher reflectance to MIR resulting in higher NDBI (Gao, 1996). Therefore, considering dry vegetation in barren land in higher hills and possibly due to soil characteristics in low land, bare soil areas exhibited higher NDBI values.

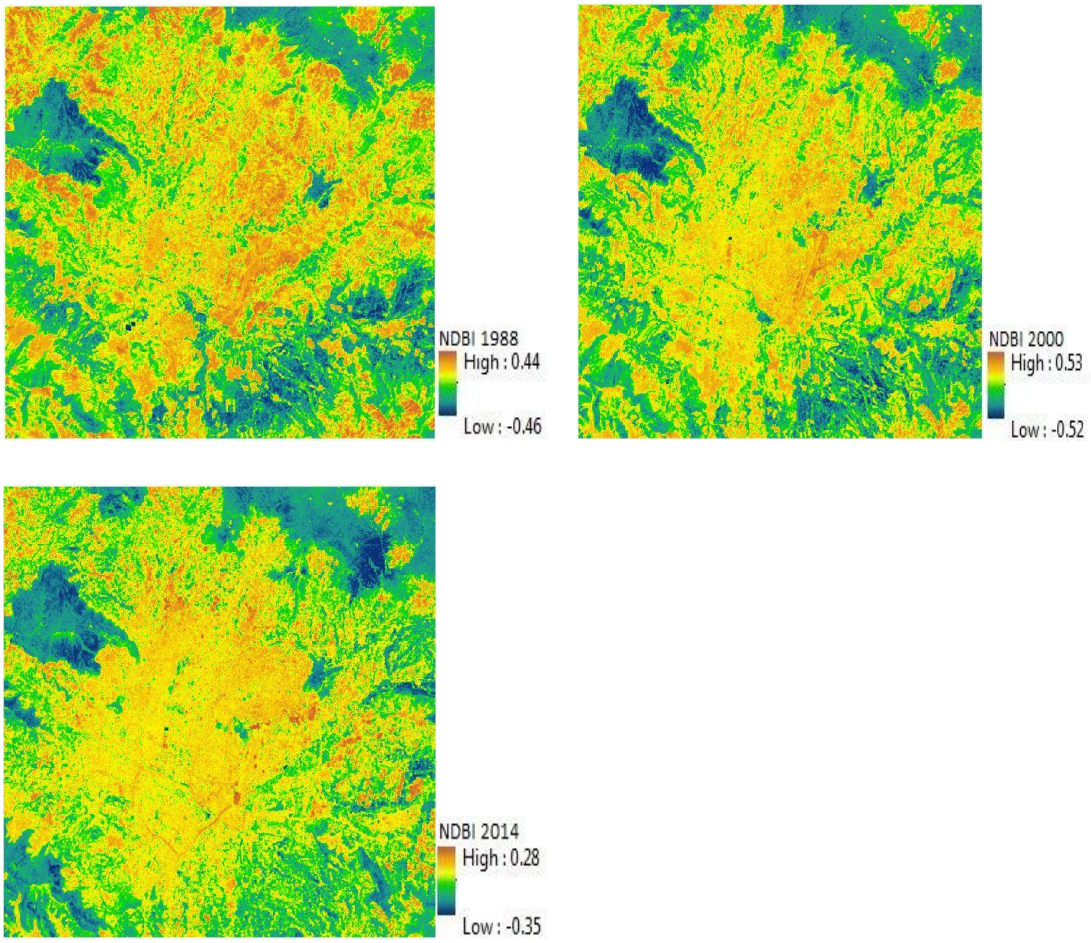

Figure 17: NDBI within each LULC class in 1988, 2000 and 2014

Figure 18 shows the graph of mean NDBI within each LULC class for 1988, 2000 and 2014. In general the NDBI values were low for most of the LULC classes. Water has the lowest NDBI value (-0.10 to -0.19). After Water, Forest and Agriculture have the low NDBI values (-0.17 to -0.09). Open area also shows quite low NDBI value (0.01 to 0.04). On the other hand, Bare soil and Urban LULC classes have substantially high NDBI values ranging from 0.12 to 0.22.

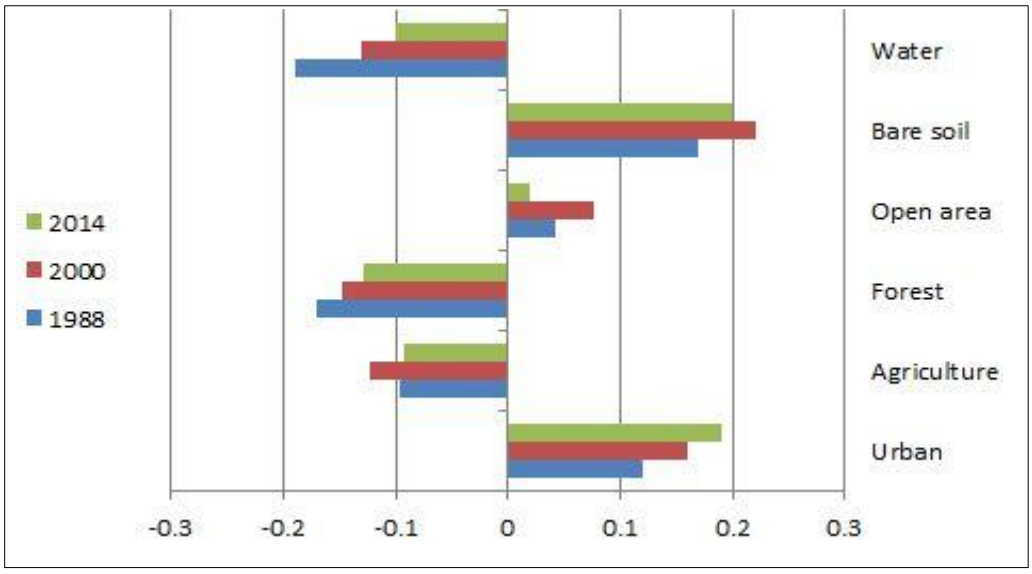

Figure 18: Mean NDBI value for each LULC class in 1988, 2000 and 2014

4.2.4 Normalized Difference Water Index

Figure 19 shows the spatial distribution of NDWI in the study area. Most of the LULC classes received low NDWI value. As expected, Water got the highest NDWI value in all three years whereas Bare soil got the lowest NDWI. Regarding Forest LULC class, though the mean NDWI value is highly negative, some portion of Forest which is shadowed due to relief and consisting of moist soil showed quite high NDWI value. It can also be observed that the range of NDWI value slightly increases from the year 1988 to 2000 and then sharply decreases in 2014.

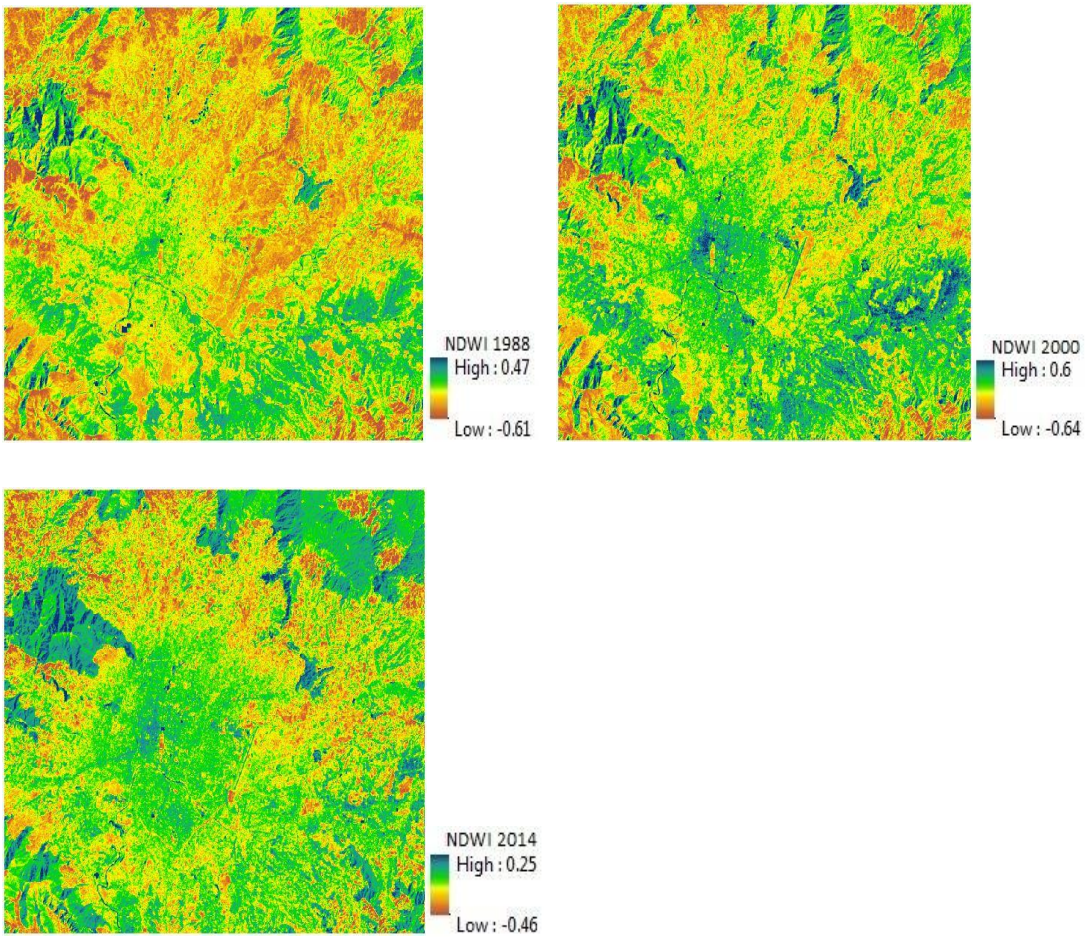

Figure 19: NDWI within each LULC class in 1988, 2000 and 2014

Figure 20 is a bar chart showing mean NDWI value within each LULC class for the years 1988, 2000 and 2014. As observed, Water is the only LULC class with positive NDWI value ranging from 0.15 to 0.22. Bare soil, Urban and Open area demonstrated highly negative NDWI (-0.19 to -0.42). Forest and Agriculture are the next LULC classes with lower NDWI value after them.

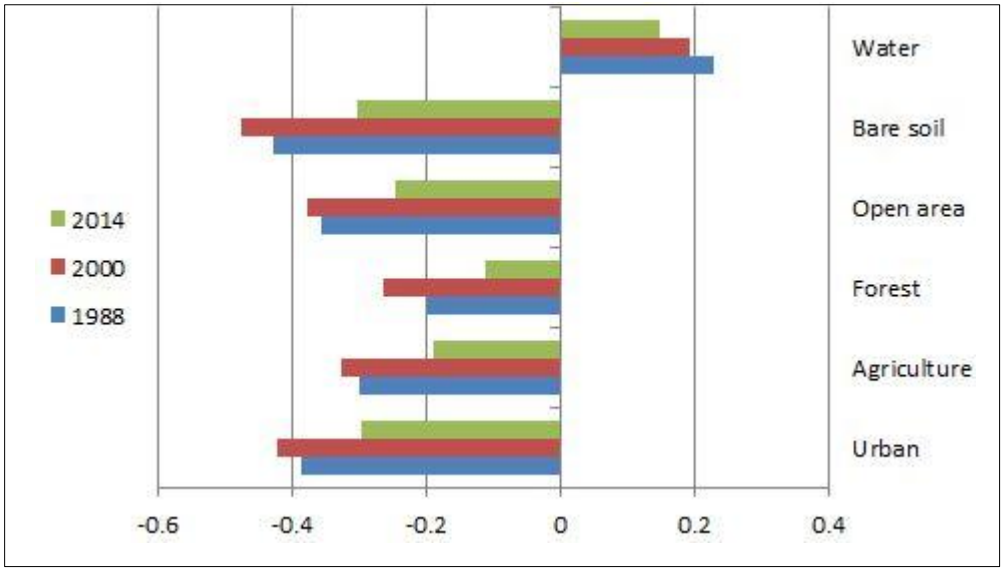

Figure 20: Mean NDWI within each LULC class in 1988, 2000 and 2014

4.3 Relationship between LST & LULC characteristics

4.3.1 Linear Regression of LST and LULC indices

To assess the relationship between LST and LULC indices, we computed their correlation. NDVI, NDBI and NDWI were the land use land cover indices used for this purpose. Since temperature can be influenced by the elevation as well, DEM was also added to the computation. The result shows that the correlation between LST and NDBI is significantly positive whereas the correlations between LST and NDVI, NDWI are significantly negative. However, the value of correlation coefficient is slightly negative in case of DEM (Table 8). This indicates that within the study area, built up area contributes to the increase in the LST while vegetation and water content have opposite effect. The influence of elevation is negative but quite low. This illustrates the importance of vegetation in the mitigation of UHI effect.

Table 8: Correlations between LST and LULC indices and DEM

April 3, 1988

	LST	NDVI	NDBI	NDWI	DEM
LST	1.000	-0.716	0.822	-0.734	-0.219
NDVI	-0.716	1.000	-0.897	0.502	0.279
NDBI	0.822	-0.897	1.000	-0.819	-0.169
NDWI	-0.734	0.502	-0.819	1.000	-0.009
DEM	-0.219	0.279	-0.169	-0.009	1.000

April 4, 2000

	LST	NDVI	NDBI	NDWI	DEM
LST	1.000	-0.718	0.806	-0. 564	-0.325
NDVI	-0.718	1.000	-0.884	0.278	0.459
NDBI	0.806	-0.884	1.000	-0.658	-0.301
NDWI	-0.564	0.278	-0.658	1.000	-0.048
DEM	-0.325	0.459	-0.301	-0.048	1.000

April 11, 2014

	LST	NDVI	NDBI	NDWI	DEM
LST	1.000	-0.742	0.839	-0. 570	-0.669
NDVI	-0.742	1.000	-0.805	0.238	0.533
NDBI	0.839	-0.805	1.000	-0.747	-0.485
NDWI	-0.570	0.238	-0.747	1.000	0.205
DEM	-0.669	0.533	-0.485	0.205	1.000

A multiple regression between LST and the indices was then generated for each year, which is assumed to be useful for monitoring the thermal environment based on LULC and terrain. The regression models developed in the study are defined below:

$$LST = -14.79NDVI + 5.40NDBI - 22.56NDWI - 0.001DEM + 22.02 \quad (1988)$$

$$LST = -6.70NDVI + 7.47NDBI - 9.69NDWI - 0.001DEM + 24.81 \quad (2000)$$

$$LST = -11.80NDVI + 6.99NDBI – 11.08NDWI - 0.004DEM + 33.02 \quad (2014)$$

where, the unit of LST is degree Celsius, and the unit of DEM is meters.

Table 9 shows the coefficients, standard error, t statistic, P-value and coefficient of determination (R^2). The high value of coefficient of determination for all three years indicates strong linear relationship of the regression models in general. Moreover, P-value for all predictors in all cases approximately equal to zero indicates that the predictors are meaningful additions to the generated models. In 1988, high magnitude of coefficients of NDVI and NDWI indicates their greater contribution to LST. In 2000, the contribution of NDVI, NDBI and NDWI are almost in the similar magnitude. However, the contribution of NDVI and NDWI are slightly greater than NDBI in 2014. The contribution of DEM in all three years is low in comparison to the LULC indices.

Table 9: Regression Analysis Parameters

April 3, 1988

	Estimate	**Std. error**	**t value**	**P value**	**R^2**
Constant	22.02	0.24	90.01	0.00	0.71
NDVI	-14.79	1.38	-10.69	0.00	
NDBI	-5.40	1.66	-3.25	0.00	
NDWI	-22.56	1.47	-15.28	0.00	
DEM	-0.001	0.00	-9.95	0.00	

April 4, 2000

	Estimate	**Std. error**	**t value**	**P value**	**R^2**
Constant	24.81	0.25	98.10	0.00	0.67
NDVI	-6.70	1.05	-6.35	0.00	
NDBI	7.47	1.23	6.05	0.00	
NDWI	-9.69	1.03	-9.32	0.00	
DEM	-0.001	0.00	-7.94	0.00	

April 11, 2014

	Estimate	**Std. error**	**t value**	**P value**	**R^2**
Constant	33.02	0.17	192.89	0.00	0.80
NDVI	-11.80	1.35	-8.72	0.00	
NDBI	6.99	1.59	4.38	0.00	
NDWI	-11.08	1.41	-7.84	0.00	
DEM	-0.004	0.00	-34.56	0.00	

To verify the developed regression models graphically, we plotted scatterplot of the measured (original) LST against estimated LST obtained from the model. Figure 21 shows the scatterplots for the three different years where it can be seen that the points tend to cluster in the linear fashion in the central region of the plot. The points are highly clustered in the year 2014 in comparison to the rest of the years. Therefore considering determination coefficient and visual examination of the scatterplot, the models seem to be satisfactory.

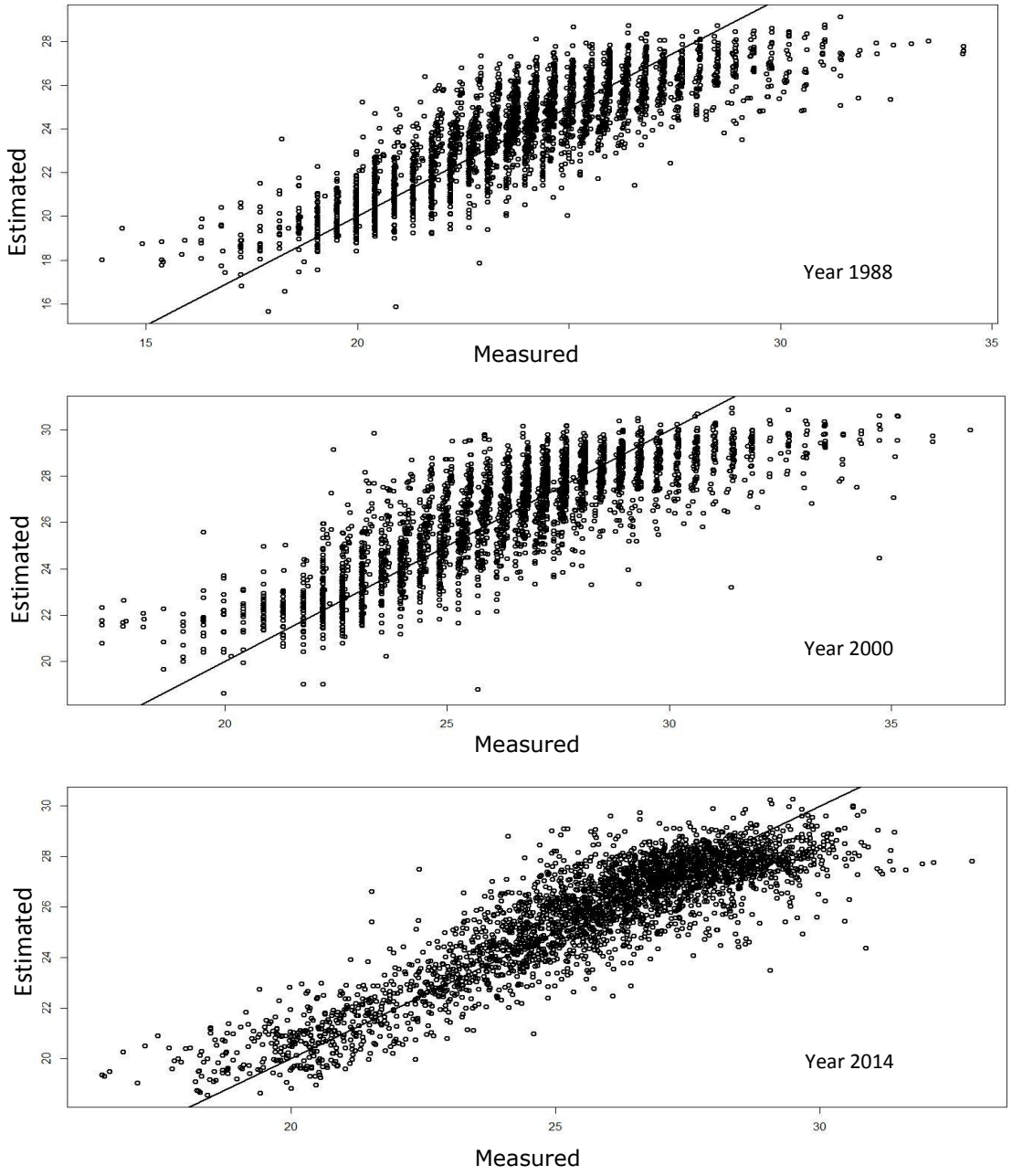

Figure 21: Measured LST vs Estimated LST for developed regression models

4.3.2 Linear Regression of LST and LULC class

We further developed regression models for each LULC class to understand its relation to LST comprehensively. Table 10 shows regression models for each LULC class in the study area for all three years. From the table we can notice that Open area LULC class has greater coefficient of determination in 1988, Bare soil in 2000 and Forest in 2014. Water has the lowest coefficient of determination in the year 1988 and 2014. In 2000 Urban LULC class showed the lowest value.

Table 10: Regression equations for each LULC class

April 3, 1988

LULC	Regression equations	R^2
Urban	-0.4NDVI + 16.06NDBI + 12.85NDWI + 0.01DEM + 7.74	0.45
Agriculture	4.94NDVI + 12.57NDBI + 3.08NDWI - 0.001DEM + 22.44	0.43
Forest	-7.65NDVI - 4.49NDBI - 16.10NDWI - 0.003DEM + 24.10	0.49
Open area	-10.27NDVI - 4.78NDBI - 19.68NDWI + 0.004DEM + 13.31	0.59
Bare soil	0.19NDVI + 7.85NDBI - 8.50NDWI + 0.01DEM + 3.39	0.35
Water	-6.05NDVI - 2.14NDBI – 3.31NDWI + 0.004DEM + 17.13	0.15

April 4, 2000

LULC	Regression equations	R^2
Urban	-16.95NDVI – 7.97NDBI – 7.74NDWI + 0.03DEM – 12.05	0.21
Agriculture	1.72NDVI + 11.49NDBI + 3.90NDWI - 0.006DEM + 16.57	0.36
Forest	-13.88NDVI - 15.77NDBI - 25.28NDWI - 0.002DEM + 23.14	0.45
Open area	-3.32NDVI + 2.49NDBI – 10.28NDWI + 0.001DEM + 20.76	0.31
Bare soil	-10.09NDVI – 2.26NDBI - 18.20NDWI + 0.007DEM + 3.39	0.47
Water	-29.44NDVI - 19.12NDBI - 22.64NDWI - 0.004DEM + 31.72	0.38

April 11, 2014

LULC	Regression equations	R^2
Urban	-3.54NDVI + 20.33NDBI + 16.58NDWI + 0.007DEM +20.48	0.44
Agriculture	-10.55NDVI - 1.58NDBI - 12.10NDWI - 0.002DEM + 29.44	0.39
Forest	1.60NDVI – 1.51NDBI – 15.06NDWI - 0.004DEM + 27.17	0.66
Open area	-7.33NDVI + 2.22NDBI – 17.83NDWI - 0.002DEM + 28.49	0.55
Bare soil	-3.81NDVI + 4.54NDBI - 8.64NDWI - 0.001DEM + 24.20	0.19
Water	-4.69NDVI + 3.90NDBI – 5.39NDWI + 0.002DEM + 23.49	0.13

In summary, the relationship between LST and LULC indices varies depending upon the LULC class. The obtained results showed some anomalies in relation to the different trends observed for the same LULC class. For instance, NDBI positively affected LST in 1988 and 2014 for urban LULC class but its effect is negative in 2000. One possible reason might be due to the multi-collinearity effect by the use of many predictors in the linear regression. Hence we recommend that linear regression can be useful to explore the general relationship between LST and LULC. However it may not be always the suitable choice particularly when we are interested to explore the relationship in depth, considering many LULC variables. Therefore, we decided to apply Kernel Ridge Regression for further analysis.

4.3.3 Assessment of LULC indices and LULC class based approach for LST prediction

We commenced our assessment procedure with the linear regression models based on LULC indices developed in the above section. We used the linear regression model of the years 1988 and 2000 to generate estimated LST for the consecutive year 2014. Measured LST data of the year 2014 was used as test sample during the process. Then we computed RMSE between the test sample and estimated LST obtained from the model as shown in the following table. As the obtained RMSE values are high, linear regression model seems to be not suitable for the purpose of use for the LST prediction.

Table 11: RMSE values for LULC indices and linear regression case

Linear Regression	Test Sample	RMSE
1988	2014	5.49
2000	2014	2.27

After that we switched on to the non-linear Kernel Ridge Regression (KRR). KRR was trained using the LULC indices and corresponding LST data of the years 1988 and 2000 to produce estimated LST for the consecutive year 2014. Then we

computed the RMSE between the test sample and the obtained estimated LST, as shown in the following table. This time, the obtained RMSE values are better than the previous ones obtained through the linear regression.

Table 12: RMSE values for LULC indices and KRR case

Training Sample	Test Sample	RMSE
1988	2014	1.37
2000	2014	1.26

Next we tested LULC class based approach with KRR. As mentioned earlier, we obtained LST and corresponding LULC proportion data at different window sizes 5*5 10*10 and 20*20. Therefore we computed RMSE values for each window case. Initially KRR was trained with 1988 and 2000 data. Then we obtained estimated LST for the year 2014 based on the training samples of 1988 and 2000 for all 5*5, 10*10 and 20*20 window cases. The RMSE was then determined between the test samples and obtained estimated LST for the year 2014 as follows.

Table 13: RMSE values for LULC class and KRR case

Training Sample	Test Sample	Window size	RMSE
1988	2014	5*5	1.90
1988	2014	10*10	1.86
1988	2014	20*20	1.78
2000	2014	5*5	1.88
2000	2014	10*10	1.54
2000	2014	20*20	1.41

Comparing the RMSE values we can conclude that LULC indices based approach using recent training sample is more suitable for the future LST prediction of the study area. Applying KRR for LULC indices of 2000 to predict LST for the year 2014 yielded the lowest RMSE of 1.26 between the test sample and the estimated LST for that year. Figure 22 depicts the scatterplot between measured and estimated LST for this particular case.

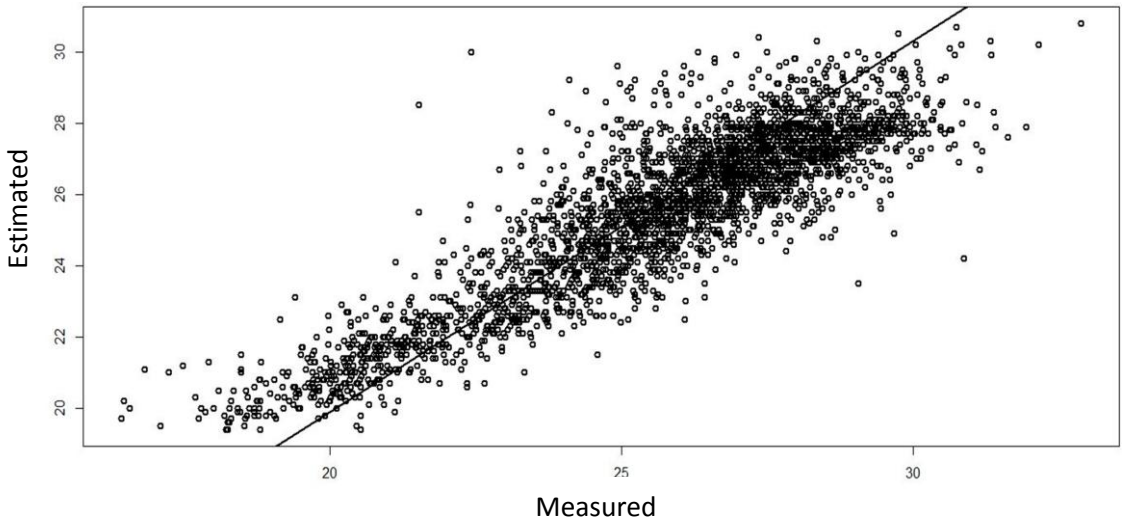

Figure 22: Measured LST vs. Estimated LST for LULC indices and KRR case for 2000

4.4 Impact of urban growth on UHI effect

Getis-ord Gi* Statistics was applied to the LST dataset to detect the presence of hot or cold spots over the study area. This is considered to be an effective approach to visualize the effect of urban heat island (Goswami et al., 2013). By this method, we are concerned with the thermal pattern rather than the absolute value of mean surface temperature. It should also be noted that the identification of hot or cold spots by this method does not necessarily imply the mean surface temperature being high or low. Figure 23 shows the Hot Spot maps of the study area for the three different dates.

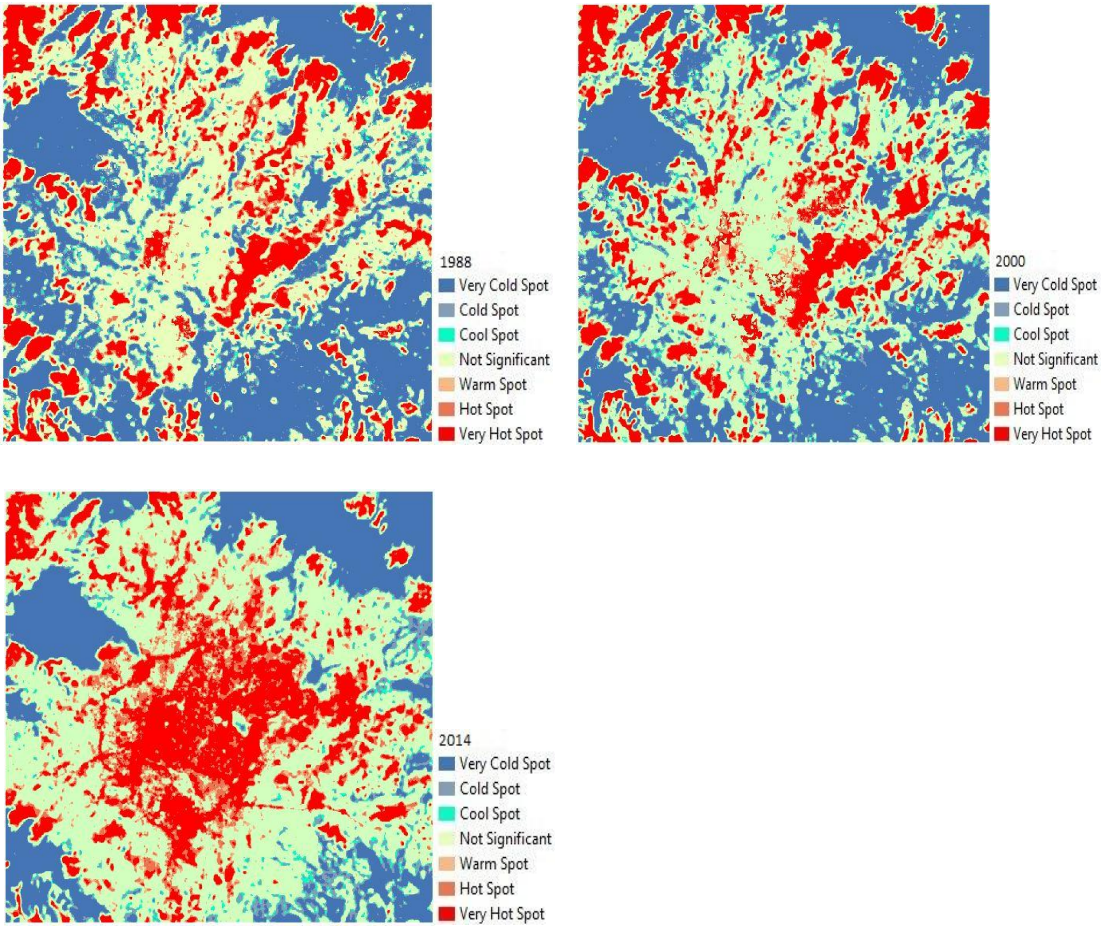

Figure 23: Hot Spot Analysis for LST in different years

The maps for the year 1988 and 2000 primarily show heat island in the airport area and the core urban area. However there is a dramatic change in the year 2014. There is a formation of big heat island covering almost the whole urban area in that year. There is a gradual removal of cold region in the central region during the period 1988-2000. The cold region is observed in the areas of high vegetation cover such as forest, open areas and agriculture. This justifies the importance of vegetation in minimizing the urban heat island effect.

Tables 14-16 show the percentage distribution of different thermal types over various LULC classes. In other words, they show the contribution of various LULC types in the spatial distribution of thermal pattern. Generally cold region is observed to occupy the greater area than hot region. However in the year 2014, hot region superseded cold region. Not-significant region also occupies large portion in our

study area. Though the contribution of urban area in the very hot region was minimal in the year 1988 and 2000, it increased by around 8% in the year 2014. Forest and Agriculture are the coldest LULC types. Figure 24 shows the LULC distribution specifically in the Hot Spot area that is the area observed to be the hot spot at 99% confidence level. Dominant land use observed in the Hot Spot area is Open area in the first two years, but it is superseded by the Urban area in 2014. It can be stated that the Urban area showed more impact on Hot Spot over time in the study area.

Table 14: Proportion of various thermal region in different LULC in 1988 (%)

LULC	Very cold	Cold	Cool	Not Sig.	Warm	Hot	Very Hot
Urban	0.328	0.398	0.291	3.913	0.162	0.210	0.447
Agriculture	15.192	1.755	0.737	2.133	0.011	0.009	0.005
Forest	12.345	0.559	0.252	0.998	0.026	0.033	0.034
Open area	5.035	3.020	1.845	20.716	1.335	2.201	8.439
Bare soil	0.305	0.292	0.224	7.206	0.859	1.644	4.844
Water	0.653	0.224	0.133	1.049	0.035	0.032	0.047
Total	33.860	6.251	3.485	36.018	2.431	4.132	13.819

Table 15: Proportion of various thermal region in different LULC in 2000 (%)

LULC	Very Cold	Cold	Cool	Not Sig.	Warm	Hot	Very Hot
Urban	0.106	0.127	0.122	6.450	0.642	0.708	1.775
Agriculture	11.416	2.228	1.044	4.837	0.057	0.064	0.068
Forest	13.005	0.445	0.152	0.654	0.009	0.007	0.008
Open area	5.374	2.583	1.693	23.208	1.798	2.730	7.867
Bare soil	0.066	0.072	0.047	2.249	0.433	0.887	5.053
Water	0.537	0.185	0.092	0.962	0.048	0.078	0.095
Total	30.506	5.642	3.152	38.363	2.988	4.476	14.869

Table 16: Proportion of various thermal region in different LULC in 2014 (%)

LULC	Very cold	Cold	Cool	Not Sig.	Warm	Hot	Very Hot
Urban	0.000	0.0003	0.001	6.129	1.987	4.031	8.475
Agriculture	1.602	2.018	1.287	15.521	0.439	0.460	0.283
Forest	13.713	0.387	0.127	0.264	0.001	0.001	0.0003
Open area	3.332	1.467	0.896	17.350	1.893	3.122	5.579
Bare soil	0.0002	0.005	0.008	1.920	0.599	1.368	3.839
Water	0.014	0.057	0.048	1.073	0.122	0.192	0.371
Total	18.663	3.937	2.370	42.259	5.043	9.175	18.549

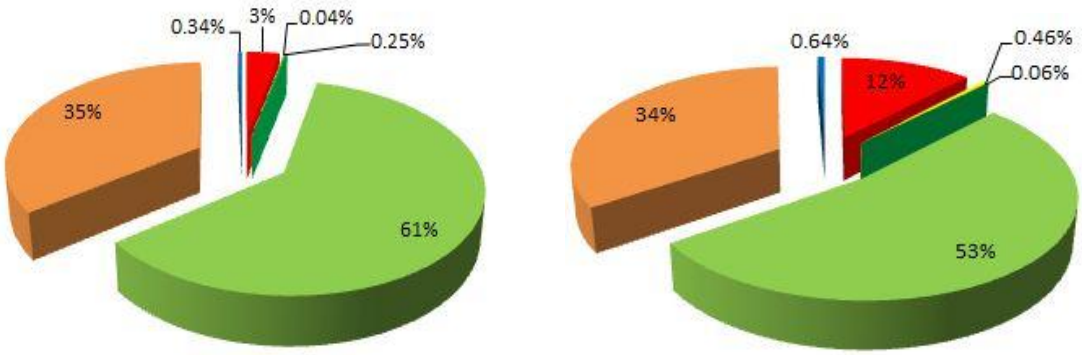

a) Year: 1988 b) Year: 2000

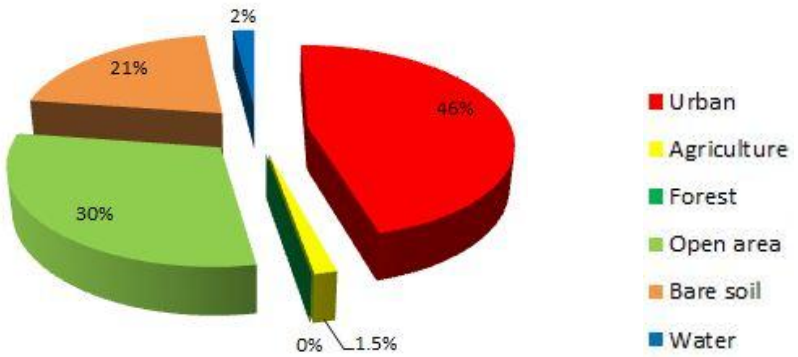

c) Year: 2014

Figure 24: LULC distribution (% area) in Hot Spot area

We know that urban growth causes urban landscape changes. Therefore it is important to relate urban landscape to the land surface temperature to understand how urban fragmentation causes the UHI effect. Table 17 shows that urban built-up is the hottest landscape type whereas rural open area is the coldest landscape type. The spatial pattern of LST can be visualized from the table as we transit through the different zones from the hottest urban built-up landscape type to the coldest rural open area landscape type, which helps us to visualize the UHI formation in the study area. Moreover, the lower LST of urbanized open area in comparison to urban built-up and suburban built-up indicates the importance of open space such as parks and other recreational areas to minimize the UHI effect.

Table 17: Mean LST by urban landscape in degree Celsius

Urban landscape	1988	2000	2014
Urban built-up	26.92	28.98	28.67
Suburban built-up	26.10	27.89	27.84
Rural built-up	25.90	27.13	26.95
Urbanized open land	25.90	27.56	27.11
Rural open land	24.74	26.19	25.88

Table 18 shows the mean LST for each urban growth type during different development periods. Infill growth has the maximum mean LST whereas Leapfrog has the minimum mean LST in all periods. This is because infill area is usually surrounded by the built-up area itself having high LST value which positively influences the LST of infill area, while leapfrog area is surrounded by the other LULC types such as open area, agriculture etc. having low LST value, which negatively influences the LST of leapfrog area.

Table 18: Mean LST by urban growth type in degree Celsius

Urban growth type	1988-2000	2000-2014	1988-2014
Infill	28.00	28.08	28.17
Extension	27.75	27.26	27.51
Leapfrog	27.30	27.04	27.13

To explore the impact of urban growth on land surface temperature, we applied linear regression to analyze the relationship between urban land cover and surface temperature. Using zonal statistics tool in ArcGIS we determined the mean LST at each percentage of urban cover from 0% to 100%. Figure 25 shows the linear regression models for the three different years. The regression models indicate that for every 1% increase in urban area, there will be increase in mean LST by 0.012^0C in 1988, 0.026^0C in 2000 and 0.039^0C in 2014 respectively.

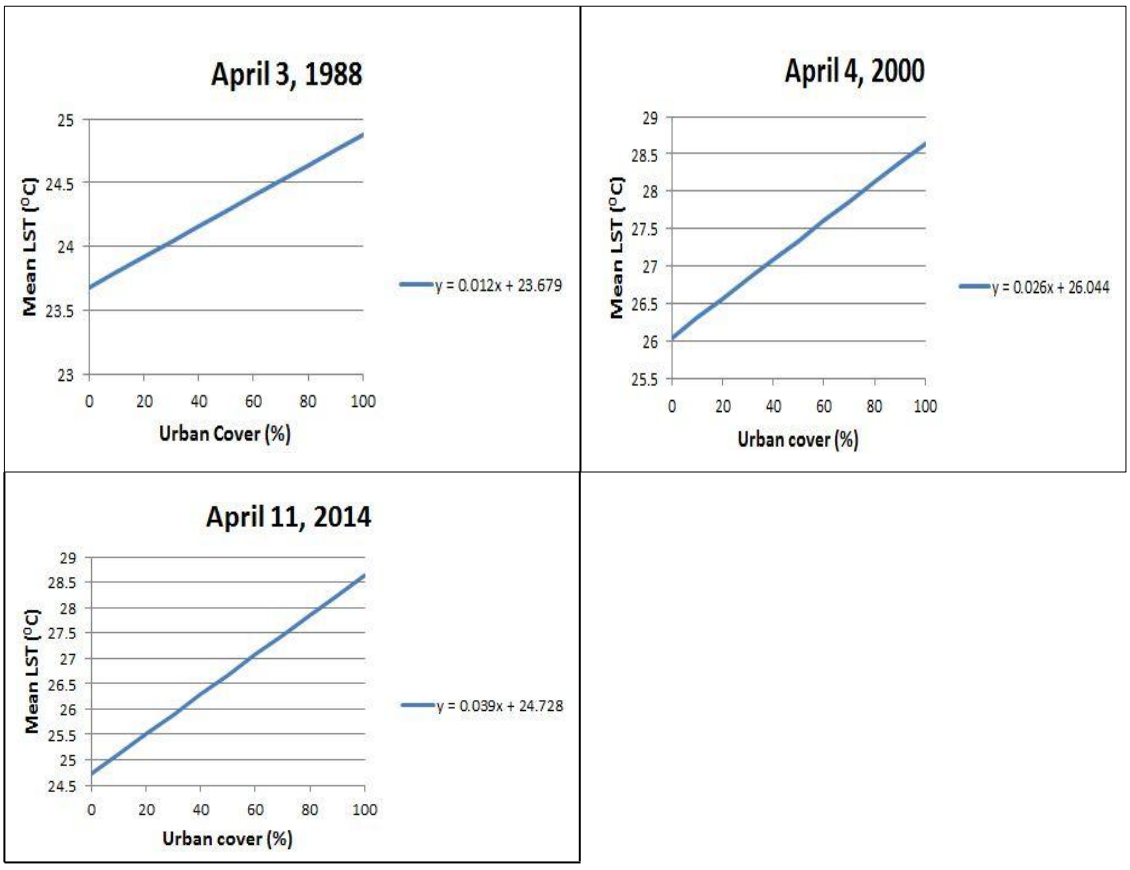

Figure 25: Linear regression between urban cover and LST

5. CONCLUSION

The study revealed high rate of urban growth in Kathmandu valley. The main drivers of such growth are high population influx and improper land use plan. As a result, productive agricultural land, open area are being replaced by the concrete structures. This trend is expected to be more severe in future unless proper land use plans and policies are implemented. Various types of urban growth such as infill, extension and leapfrog were found to exist in the valley. However, infill type of urban growth is more hazardous in the sense that it fills up existing open area making cities congested and the consequences of such growth were apparent during Nepal Earthquake 2015, when many people lose their lives due to inaccessibility to the safe open places for emergency evacuation.

Based on our analysis of thermal pattern of the study area over the given period of time, we found gradual increase in temperature in urban area. There was the formation of urban heat island in the central urban area of the valley. The study proved that the surface temperature is influenced by the urban growth. Urban growth not only increases the UHI effect but also affects quality of life of the people residing in the urban area.

We also explored the relationship between LST and LULC through regression analysis. The results indicated strong linear relationship between surface temperature and LULC indices. We then performed regression analysis between LST and LULC indices for each LULC class. This exhibited variations in the relationship depending upon the LULC types. Regarding determination of the appropriate approach for LST prediction, we compared LULC indices and LULC class based methods and found that LULC indices method gives better prediction in comparison.

However there were some limitations in the study. The resolution of the images was just moderate for classification and change detection purpose. Despite of massive repository of Landsat imagery, sometimes it is difficult to get the suitable images as per our requirement. In addition, due to spectral mixing of different land cover within the pixels and complex landscape of the study area, pixel based classification did not give us higher accuracy. Likewise our study focused on LST pattern rather than its

absolute value over the area of interest. Furthermore, our study is primarily based on daytime LST during summer season considering only three years.

Hence we recommend that as urban growth in Kathmandu valley is in critical condition it is high time that concerned authorities take necessary initiatives and urban residents develop resilience to urban growth and UHI effect. We also recommend using high resolution images and other classification method so that more LULC classes at higher accuracy can be obtained. To obtain robust results for LULC-LST relationship it is better to take into account both daytime and nighttime temperature data for more years. Similarly, if absolute temperature is also to be prioritized then atmospheric correction parameters considering local climatic parameters has to be applied. Last but not the least we need to assess other regression methods as well to understand the LULC-LST relationship in depth.

REFERENCES

ADB/ICIMOD. (2006). *Environment Assessment of Nepal: Emerging Issues and Challenges*.Kathmandu: ICIMOD.

Adhikary, D. (2015). *2015 Nepal Earthquake – A Geological and Geotechnical Perspective and Implications to Kathmandu Valley*. Last visit 1/7/2017, https://dpadhikary.wordpress.com/tag/kathmandu-soil

Ahmed, B., Kamruzzaman, M., Zhu, X., Rahman, M.S., & Choi, K. (2013). Simulating Land Cover Changes and Their Impacts on Land Surface Temperature in Dhaka, Bangladesh. *Remote Sensing,* 5, 5969-5998.

Angel, S., Parent, J., & Civco, D.L. (2012). The fragmentation of urban landscapes: global evidence of a key attribute of the spatial structure of cities, 1990–2000. *Environment and Urbanization, 24(1), 249-283.*

Artis, D.A., Carnahan, W.H. (1982). Survey of emissivity variability in thermography of urban areas, *Remote Sensing of Environment*. 12(4), 313–329.

Baniya, N. (2008). *Land Suitability Evaluation Using GIS for Vegetable Crops in Kathmandu Valley/Nepal*. Last visit 1/6/2017, http://edoc.hu-berlin.de/dissertationen/baniya-nabarath-2008-10-13/PDF/baniya.pdf

Bekele, H. (2005). *Urbanization and Urban Sprawl.* Master thesis, Department of Infrastructure Section of Building and Real Estate Economics, Kungliga Tekniska Högskolan, Stockholm, Sweden.

Central Bureau of Statistics (CBS portal, 2017). http://www.cbs.gov.np

Chavez, P.S. (1996). *Image-Based Atmospheric Corrections – Revisited and Improved, Photogrammetric Engineering & Remote Sensing*. 62(9), 1025-1036.

Chen, X., Zhao, H., Li, P., & Yin, Z. (2006). Remote sensing image-based analysis of the relationship between urban heat island and land use/cover changes. *Remote Sensing of Environment,* 104(2), 133-146.

Cibula, W.G., Zetka, E.F. & Rickman, D.L. (1992). Response of thematic mapper bands to plant water stress. *International Journal of Remote Sensing*, 13, 1869-1880.

Congalton, R. & Green, K. (1999). *Assessing the accuracy of remotely sensed data. Principles and practices.* Lewis Publishers, Boca Raton, Florida.137p.

Coseo, P., & Larsen, L. (2015). Cooling the Heat Island in Compact Urban Environments: The Effectiveness of Chicago's Green Alley Program. *Procedia Engineering, 118, 691-710.*

DoR. (2004). *List of Important Roads and Status*. Road Statistics, Kathmandu: Government of Nepal. Last visit 1/4/2017, https://www.dor.gov.np/road_statistic_2004/list_of_important_roads.php

ESRI. (2016). *How Hot Spot Analysis (Getis-Ord Gi*) works*, Last visit 17/10/2016, http://pro.arcgis.com/en/pro-app/tool-reference/spatial-statistics/h-how-hot-spot-analysis-getis-ord-gi-spatial-stati.html

Fabrizi, R., Bonafoni, S., & Biondi, R. (2010). Satellite and ground-based sensors for the urban heat island analysis in the City of Rome. *Remote Sensing*, *2*, 1400–1415.

Foody, G. (2002). Status of land covers classification accuracy assessment, *Remote Sensing of Environment*, 80, 185-201.

Gao, B.C. (1996). NDWI–A normalized difference water index for remote sensing of vegetation liquid water from space, Remote Sensing of Environment, 58(3), 257–266.

Ghimire A.B., & Upreti, B.R. (2008). Conflict Induced Displacement: An emerging phenomenon of Internal Migration in Nepal. In Pyakuryal, K.N., Upreti, B.R., & Sharma, S.R. (Eds.), *Nepal: Transition to Transformation* (pp. 101-140). Kathmandu University: Human and Natural Resources Studies Center & NCCR North South: South Asia Regional Coordination Office.

Goswami, J., Roy, S., & Sudhakar, S. (2013). A Novel Approach in Identification of Urban Hot Spot Using Geospatial Technology: A Case Study in Kamrup Metro District of Assam, *Internation Journal of Geosciences*, 4, pp. 898-903.

Goward, S.N. (1981). THERMAL BEHAVIOR OF URBAN LANDSCAPES AND THE URBAN HEAT ISLAND. *Physical Geography*, 2(1), 19-33.

Grimmond, S. (2007). Urbanization and global environmental change: local effects of urban warming. *The Geographical Journal*, 173(1), 83-88.

Guo, G., Wu, Z., Xiao, R., Chen, Y., Liu, X., & Zhang, X. (2015). Impacts of urban biophysical composition on land surface temperature in urban heat island clusters. *Landscape and Urban Planning, 135, 1-10.*

Higgins, J. (2005). *The Radical Statistician.* Last visit, 1/10/2017, http://www.biddle.com/documents/bcg_comp_chapter4.pdf

Imhoff, M.L., Zhang, P., Wolfe, R.E., & Bounoua, L. (2010). Remote sensing of the urban heat island effect across biomes in the continental USA. *Remote Sensing of Environment,* 114(3), 504-513.

Kathmandu Valley in Nepal. (Tourism portal, 2017). http://www.welcomenepal.com/places-to-see/kathmandu-valley.html

Katuwal, H.B., Bhandari, J., Thapa, V., Gurung, R., Chaudhary, R., Magar, T.G., & Chaudhary, H. (2016). How many birds do the sacred forests hold? *The Journal of Zoology Studies*, 3(4), 7-19.

Kim, J.P., & Guldmann, J.M. (2014). Land-Use Planning and the Urban Heat Island. *Environmental and Planning B: Planning and Design*, 41(6), 1077-1099.

Landsat, N. A. S. A. (7). *Science Data Users Handbook. 2011*, Last visit 9/23/2016, http://landsathandbook.gsfc.nasa.gov/inst_cal/prog_sect8_2.html.

Landsat, N. A. S. A. (8). *Science Data Users Handbook. 2015*, Last visit 10/18/2016 http://landsat.usgs.gov/l8handbook.php.

Li, K., Lin, B., Jiang, D. (2012). A New Urban Planning Approach for Studying Heat Islands at the Community Level. *Journal of Heat Island Institute*, 7(2), 50-54.

Lillesand, T., Keifer, R.W., & Chipman, J. (2007). *Remote Sensing and Image Interpretation* (Sixth Edition), Wiley, Hoboken, USA.

Lo, C.P., & Quattrochi, D.A. (2003). Land-Use and Land-Cover Change, Urban Heat Island Phenomenon, and Health Implications. *Photogrammetric Engineering & Remote Sensing*, 9, 1053-1063.

Mirzaei, P. A. (2015). Recent challenges in modeling of urban heat island. *Sustainable Cities and Society*, 19, 200-206.

Oke, T. R. (1982). The energetic basis of the urban heat island. *Quarterly Journal of Royal Meteorological Society*, 108, 1–24.

Pant, P. R., Dongol, D. (2009*). Kathmandu Valley Profile*, *Briefing Paper*. Last visit 1/6/2017, http://www.eastwestcenter.org/fileadmin/resources/seminars/Urbanization_Seminar/Kathmandu_Valley_Brief_for_EWC___KMC_Workshop__Feb_2009.pdf

Parker, D. E. (2010). Urban heat island effects on estimates of observed climate change. *Wiley Interdisciplinary Reviews: Climate Change*, 1(1), 123–133.

Piya, B.K. (2004). *Generation of a Geological database for Liquefaction hazard assessment in Kathmandu valley*. Master thesis, International Institute for Geo-information Science and Earth Observation, ITC, Enschede, Netherlands.

Qin, Z., Karnieli, A., & Berliner, P. (2001). A mono-window algorithm for retrieving land surface temperature from Landsat TM data and its application to the Israel-Egypt border region. *International Journal of Remote Sensing*, 18, 3719-3746.

Quattrochi, D. A., & Luvall, J. C. (1999). Thermal infrared remote sensing for analysis of landscape ecological processes: methods and applications.*Landscape ecology*, 14(6), 577-598.

Rimal, B. (2011).Urban Growth and Land use/Land cover change of Pokhara Sub-Metropolitan city, Nepal. *Journal of Theoretical and Applied Information Technology*, 26(2), 118-129.

Rizwan, A.M., Dennis, L.Y.C., & Liu, C. (2008). A review on the generation, determination and mitigation of Urban Heat Island. *Journal of Environmental Sciences*, 20(1), 120-128.

Rosipal, R., & Trejo, L.J. (2001). *Kernel Partial Least Squares Regression in Reproducing Kernel Hilbert Space*, Last visit 1/10/2017, http://www.jmlr.org/papers/volume2/rosipal01a/rosipal01a.pdf

Rouse Jr, J., Haas, R. H., Schell, J. A., & Deering, D. W. (1974). Monitoring vegetation systems in the Great Plains with ERTS. *NASA special publication*, 351, 309.

Sailor, D. J., & Lu, L. (2004). A top-down methodology for developing diurnal and seasonal anthropogenic heating profiles for urban areas. *Atmospheric Environment*, 38, 2737–2748.

Saitoh, T.S., Shimada, T., & Hoshi, H. (1996). Modeling and simulation of the Tokyo urban heat island. *Atmospheric Environment*, 30(20), 3431-3442.

Saunders, C., Gammerman, A., & Vovk, V. (1998). Ridge regression learning algorithm in dual variables. In *(ICML-1998) Proceedings of the 15th International Conference on Machine Learning* , 515-521.

Sharma, P. (2003). Urbanization and Development. In *Population Monograph of Nepal* (Vol. 1, pp. 375-412). Kathmandu: Central Bureau of Statistics.

Shrestha, T.K. (1998). *The Spiny Babbler*, R.K Printers, Teku, Kathmandu.

Snyder, W.C., Wan, Z., Zhang, Y., & Feng, Y.Z. (1998). Classification based emissivity for land surface temperature measurement from space, *International Journal of Remote Sensing*. 19 (14), 2753–2774.

Sobrino, J. A., Jiménez-Muñoz, J. C., & Paolini, L. (2004). Land surface temperature retrieval from LANDSAT TM 5. *Remote Sensing of environment*, 90(4), 434-440.

SRIVANIT, M., Hokao, K., & Phonekeo, V. (2012). Assessing the Impact of Urbanization on Urban Thermal Environment: A Case Study of Bangkok Metropolitan, *International Journal of Applied Science and Technology*, 2(7), 243-256.

Stewart, I. D., & Oke, T.R. (2012). Local climate zones for urban temperature studies. *American Meteorological Society*, 93, 1879–1900.

Sun, Q., Wu, Z., & Tan, J. (2012). The relationship between land surface temperature and land use/land cover in Guangzhou, China. *Environmental Earth Science*, 65, 1687-1694.

Tan, J., Zheng, Y., Tang, X., Guo, C., Li, L., Song, G., Zhen, X., Yuan, D., Kalkstein, A.J., & Li, F. (2010). The urban heat island and its impact on heat waves and human health in Shanghai. *International Journal of Biometeorology*, 54(1), 75-84.

Tempfli, K., Kerle, N., Huurneman, G.C., & Janssen, L.L.F. (2009). *Principles of Remote Sensing. An introductory textbook* (ITC Educational Textbook Series 2), Enschede, ITC.

Thapa, R.B. (2009). *Spatial Process of Urbanization in Kathmandu Valley, Nepal*. PhD. Thesis, Graduate School of Life and Environmental Sciences, University of Tsukuba, Tsukuba, Japan.

Thapa, R.B., & Murayama, Y. (2009). Examining Spatiotemporal Urbanization Patterns in Kathmandu Valley, Nepal: Remote Sensing and Spatial Metrics Approaches. *Remote Sensing*, 1, 534-556.

Tran, H., Uchihama, D., Ochi, S., & Yasuoka, Y. (2006). Assessment with satellite data of the urban heat island effects in Asian mega cities. *International Journal of Applied Earth Observation and Geoinformation*, 8(1), 34-48.

UNHABITAT. (2015). *Kathmandu Valley, Nepal – Climate Change Vulnerability Assessment*. Last visit 9/11/2016, http://unhabitat.org/books/kathmandu-valley-nepal-climate-change-vulnerability-assessment.

United Nations Office of the High Commissioner for Human Rights (UN-OHCHR). (2012). *Nepal Conflict Report.* Geneva.

Weng, Q., Lu, D., & Schubring, J. (2004). Estimation of land surface temperature–vegetation abundance relationship for urban heat island studies. *Remote Sensing of Environment,* 89(4), 467-483.

Xu, H. (2006). Modification of Normalised Difference Water Index (NDWI) to Enhance Open Water Features in Remotely Sensed Imagery. *International Journal of Remote Sensing,* 27(14), 3025-3033.

Yu, X., Guo, X., & Wu, Z. (2014). Land Surface Temperature Retrieval from Landsat 8 TIRS - Comparison between Radiative Transfer Equation-Based Method, Split Window Algorithm and Single Channel Method. *Remote Sensing,* 6, 9829-9852.

Yuan, F., & Bauer, M.E. (2007). Comparison of impervious surface area and normalized difference vegetation index as indicators of surface urban heat island effects in Landsat imagery. *Remote Sensing of Environment,* 106(3), 375-386.

Zaksek, K., & Ostir, K. (2011). Downscaling land surface temperature for urban heat island diurnal cycle analysis. *Remote Sensing of Environment,* 115, 114-124.

Zha, Y., Gao, J., & Ni, S. (2003). Use of normalized difference built-up index in automatically mapping urban areas from TM imagery, *International Journal of Remote Sensing*, 24(3), 583–594.

Zhu, S., & Zhang, G. (2011, October). Analysis on Relationship between Urban Land Surface Temperature and Landcover from Landsat Etm+ Data. In: Proc. of *Fourth International Symposium on Knowledge Acquisition and Modeling, IEEE,* Sanya, China.

APPENDICES

Landsat 4-5 Thematic Mapper (TM)	Bands	Wavelength (micrometers)	Resolution (meters)
	Band 1 - Blue	0.45-0.52	30
	Band 2 - Green	0.52-0.60	30
	Band 3 - Red	0.63-0.69	30
	Band 4 - Near Infrared (NIR)	0.76-0.90	30
	Band 5 - Shortwave Infrared (SWIR) 1	1.55-1.75	30
	Band 6 - Thermal	10.40-12.50	120* (30)
	Band 7 - Shortwave Infrared (SWIR) 2	2.08-2.35	30

* TM Band 6 was acquired at 120-meter resolution, but products are resampled to 30-meter pixels.

1. Band Designations for Landsat 4-5 Thematic Mapper (TM) (Source: USGS portal)

Landsat 8 Operational Land Imager (OLI) and Thermal Infrared Sensor (TIRS)	Bands	Wavelength (micrometers)	Resolution (meters)
	Band 1 - Ultra Blue (coastal/aerosol)	0.43 - 0.45	30
	Band 2 - Blue	0.45 - 0.51	30
	Band 3 - Green	0.53 - 0.59	30
	Band 4 - Red	0.64 - 0.67	30
	Band 5 - Near Infrared (NIR)	0.85 - 0.88	30
	Band 6 - Shortwave Infrared (SWIR) 1	1.57 - 1.65	30
	Band 7 - Shortwave Infrared (SWIR) 2	2.11 - 2.29	30
	Band 8 - Panchromatic	0.50 - 0.68	15
	Band 9 - Cirrus	1.36 - 1.38	30
	Band 10 - Thermal Infrared (TIRS) 1	10.60 - 11.19	100 * (30)
	Band 11 - Thermal Infrared (TIRS) 2	11.50 - 12.51	100 * (30)

* TIRS bands are acquired at 100 meter resolution, but are resampled to 30 meter in delivered data product.

2. Band Designations for Landsat 8 OLI (Source: USGS portal)

Masters Program in **Geospatial Technologies**

Supported by:
Education and Culture
ERASMUS MUNDUS